Improvement of Canada's hydrokinetic energy resource database

Kirby, Katelyn; Ferguson, Sean; Rennie, Colin; Nistor, Ioan; Cousineau, Julien

Publisher's version / Version de l'éditeur:
https://doi.org/10.4224/40003535
Technical Report (National Research Council Canada. Ocean, Coastal and River Engineering Research Centre); no. NRC-OCRE-2024-TR-009, 2024-03

NRC·CNRC

Improvement of Canada's Hydrokinetic Energy Resource Database

Report No.: NRC-OCRE-2024-TR-009
Date: March 2024
Authors: Katelyn Kirby, Sean Ferguson, Colin Rennie, Ioan Nistor, Julien Cousineau

Ocean, Coastal and River Engineering Research Centre

NRC.CANADA.CA

National Research Council Canada
Conseil national de recherches Canada

Canada

Summary

The purpose of this work was to improve the Canadian hydrokinetic (HK) energy database produced in 2014 using newly available data and methods. The two areas of the database that were identified to have the greatest opportunity for improvement were river width estimates and completion of the database in the Arctic. The previous database was not able to provide flow, depth, width, velocity, or power estimates in the Arctic area of Canada; thus, with newly available hydrologically and hydraulically driven flow data, this update could be achieved. Additionally, with the greatly increased availability of medium-resolution, openly accessible satellite imagery (i.e., Sentinel-2 Multispectral Instrument or S2MSI, Sentinel-1 Synthetic Aperture Radar or S1SAR, and the Landsat series), satellite imagery surface water detection methods have improved. Detecting waterbodies from space is now achievable at a 20m or 10m resolution; thus, river width can be extracted directly from imagery. The imagery used to generate river width estimates was S2MSI and the imagery was classified using the spectral index AWEI_NSH with a uniform threshold of -0.3. Imagery-derived widths were extracted in New Brunswick, Nova Scotia, and southern Gaspe (i.e., the Maritimes watershed, Watershed 1, or WS1). Additionally, river widths throughout Canada were extracted from Canada's National Hydro Network (NHN) database.

Based on comparison to highly resolved satellite images, both NHN-derived and imagery-derived widths were able to substantially improve measurements of river width from the previous 2014NRC database. NHN-derived widths may be more accurate for small rivers and imagery-derived widths are likely to be more accurate for larger rivers. Nonetheless, the imagery-derived widths are expected to improve more the river width estimates, as it was observed that the NHN polygons can under- or overestimate the river width where the NHN polygons are non-representative of current conditions. The relationship between imagery-derived width and percent flow exceedance was weak in major watershed 1 (i.e., the Maritimes watershed), so the power estimates were derived with the mean imagery-derived width and the maximum and minimum widths were used to calculate the lower and upper limits of hydrokinetic power, respectively.

The updated HK power database allows the user to locate specific cross sections of rivers that have a high potential for feasible HK power extraction, rather than the reach-averaged approach used in the 2014NRC database. It is, however, less continuous than the 2014NRC dataset as estimates of HK power in lakes and reservoirs are not included. British Columbia contained the most rivers with continuous high HK power potential where the river flow was constrained within canyons or high slope landforms. In other major watersheds, such as St. Lawrence, Northern Quebec, Labrador, and Albany, high HK power cross sections were identified and generally corresponded to a location of white water. Braided rivers and rivers located at low slope landforms were generally predicted to have low HK power, unless a width constriction was present. The flow estimates from the NRC2014 database were less representative in underfit streams when compared to historical gauge data, and the NHN polygons sometimes poorly represented waterbodies in the prairies and the Yukon where rivers had meandered from their original position, causing errors in the HK power estimates.

Planned future work to upgrade the updated HK energy database are to link the river flow estimates in the Arctic to the database points representing Arctic rivers, derive river depth estimates for Arctic rivers based on the regionalization relationships used in the previous 2014NRC database, optimize the imagery-derived widths and apply the imagery-based width estimation in the ten other major watersheds in Canada, and perform further validation on the final HK power estimates in the database by comparing the estimates with power values calculated from field data and hydrodynamic modelling.

List of Symbols

A	= River cross-sectional area [m]
$A(f)$	= River cross-sectional area corresponding to flow frequency, f [m]
a, c, k	= Hydraulic geometry coefficients
b, f, m	= Hydraulic geometry exponents
B_i	= Width on the PDC that the point represents as a decimal probability
d	= River depth [m]
$d(f)$	= River depth corresponding to flow frequency, f [m]
N_B	= Number of points on the PDC
P_i	= Theoretical power present at the point on the PDC [W]
P_K	= Hydrokinetic power [W]
Q	= Flow rate [m^3/s]
$Q(f)$	= Flow rate corresponding to flow frequency, f [m^3/s]
v	= Flow velocity [m/s]
$v(f)$	= Flow velocity corresponding to flow frequency, f [m/s]
w	= River width [m]
$w(f)$	= River width corresponding to flow frequency, f [m]
ρ	= Density of water [kg/m^3]

List of Acronyms

AEP	= Annual energy production
ASHG	= At-a-station hydraulic geometry
AWEI_NSH	= Automated Water Extraction Index, No Shadow
DHG	= Downstream hydraulic geometry
DN	= Digital number
ESA	= European Space Association
FDC	= Flow duration curve
GEM	= Global Environmental Model
GIS	= Geographic information system
HK	= Hydrokinetic
MAE	= Mean absolute error
MLC	= Maximum likelihood classifier
MLR-CCA	= Multiple linear regression coupled with canonical correlation analysis
MNDWI	= Modified Normalized Difference Water Index
NDWI	= Normalized Difference Water Index
NHN	= National Hydro Network
PDC	= Power duration curve
RMSE	= Root mean squared error
SVM	= Support vector machine
S2MSI	= Sentinel-2 Multispectral Instrument
VDC	= Velocity duration curve
WDC	= Width duration curve
WS1	= Watershed 1 in the NHN framework (i.e., Nova Scotia, Prince Edward Island, and Gaspé Peninsula)
WSC	= Water Survey of Canada
WSC-MD	= Water Survey of Canada Measurement Database

Table of Contents

List of Figures

List of Tables

1 Introduction

There is growing concern surrounding climate change and implications on weather, climate extremes, and related losses and damage [1]. These concerns have sparked initiatives at both national and international scales to reduce greenhouse gas emissions in an effort to curb human-induced climate change [2], [3]. Canada's Emissions Reduction Plan [2] outlines Canada's plan to reduce greenhouse gas emissions, including efforts to advance and apply renewable energy solutions to further alleviate reliance on fossil fuel-derived energy. In particular, there is increasing interest in run-of-river hydrokinetic (HK) energy systems that harness energy from the natural flow of river systems, without the need for damming operations.

1.1 Motivation

Canada's electricity sector is comprised of a multitude of energy resources including hydro, nuclear, coal, gas, oil, and non-hydro renewables such as wind and solar [2]. Approximately 83% of the power generation in Canada is considered to be "non-emitting" and is comprised of hydro, nuclear, and other renewable energy resources [4]. Hydro power generation harnesses energy from flowing water and provides most of the electricity generation in Canada, representing approximately 60% of Canada's total power generation [4]. Despite being a clean energy resource from an emissions perspective, large-scale hydro power operations that require significant modifications of the natural watercourse cause other environmental and societal impacts. For example, hydro power projects that require damming can alter the flow and sediment transport regime, impact fish habitat and migration, affect water quality, and have societal impacts on surrounding communities [5]–[9].

Unlike conventional hydro power generation, where a large hydraulic head difference across a turbine or series of turbines is generated via damming, "run-of-river" hydrokinetic (HK) power generation strategies harness energy from the natural flow of the river. HK energy applications are comprised of turbines deployed directly into the river without the need for damming. Consequently, HK energy applications have much less impact on the natural flow and sediment transport of the river system compared to dammed hydro power generation. By extension, HK energy applications have a relatively-lower environmental, ecological, and societal impact than dammed hydro power generation [10].

Dammed hydropower generation is generally more consistent and predictable than HK power generation owing to the anthropogenic influence and control afforded by dam structures and operations. Conversely, HK energy availability and power generation are less consistent owing to spatial and temporal fluctuations in the velocity flow field of the river. For example, optimal turbine location within a study reach may change depending on the flow conditions. Detailed analyses characterizing spatial and temporal adjustments in the flow field are required to understand implications for optimal turbine placement [11], [12]. Practitioners must also be conscious of minimum technical and operational constraints pertaining to turbine technology such as minimum required depths and cut-in speeds. The International Electrotechnical Commission has published a Technical Specification for river energy resource assessment to encourage consistency and accuracy in the determination of theoretical energy resources [13].

There is increasing interest in HK power generation in Canada owing to the abundance of surface water resources across the country as well as the environmental and societal benefits of HK power generation over dammed hydro power generation. A need was identified for improved estimates of theoretical HKE resources at the national scale to facilitate advancement of HK power generation and further alleviate reliance on fossil fuel-derived energy. In 2019, National Research Council Canada (NRC) embarked on a collaborative research project with the University of Ottawa to improve Canada's HK energy database, building from previous research completed by NRC in 2014[14]. The research was commissioned by Natural Resources Canada's (NRCan) CanmetENERGY research centre. This report summarizes the development of the new database as well as plans for future improvement.

1.2 Background and Previous Research

A detailed summary of HK energy is presented by Khaliq and Cousineau [15]. In summary, theoretical HK energy represents the energy available in flowing water. HK energy can be expressed as,

$$P_k = \frac{1}{2}\rho A v^3 \tag{1-1}$$

where P_k represents the HK energy, ρ represents the density of the fluid, A represent the cross-sectional area of the flow, and v represents the flow velocity. Readers are referred to Khaliq and Cousineau for a detailed summary of computational methods for HK energy estimation in river systems [15].

Kirby et al. [16] present an extensive review of HK energy resource assessments documented in literature at both local and regional scales, including the 2014 database of HK energy in Canadian river systems developed by Jenkinson and Bomhof [14]. Kirby et al. [16] synthesized their findings to highlight research needs and opportunities, including the potential utility of remotely sensed data to support estimation of channel geometry and discharge.

1.3 Objectives and Scope

The objective of this work was to update the 2014 national-scale HK energy database developed by Jenkinson and Bomhof [14]. This report summarizes the development of the new national-scale HK energy database, hereafter referred to as the 2014NRC database. A number of improvements were integrated into the new database including:

- Improved channel width estimates throughout Canada based on information available from the National Hydro Network (NHN) [14]
- A demonstration of improved channel width estimates derived from satellite imagery in one of eleven of Canada's major drainage basins
- Synthesizing results to provide practical summaries of HK energy resources across Canada, excluding the Arctic, based on satellite imagery-derived river width in major Watershed 1 (WS1) and based on NHN-derived river width in all major watersheds
- Restructuring of the HK database to conform to the structure of the NHN (as opposed to the now-archived Atlas of Canada 1,000,000 National Frameworks Data [17])

To meet the previously stated objective of updating the national-scale HK energy database, future work beyond the scope of this report will focus on:

- Estimates for HK energy based on flow estimates developed by Teufel and Sushama, including estimates of HK energy in the Arctic
- Estimating channel widths from satellite imagery in the remaining major drainage basins of Canada
- Synthesizing results to provide practical summaries of HK energy resources across Canada based on satellite imagery-derived river width in the remaining ten major drainage basins
- Further comparison of HK energy resource estimates with field observations and numerical modelling results [11], [12]
- Quantification of uncertainty

In order for estimates of HK energy to be developed nationally, the scope of the methods to produce the database needed to be limited [10]. The following assumptions were made in the development of the updated database:

- The impact of the HK turbine on the hydraulics of the rivers or on the power extracted from the river was not considered in the final estimates. The estimates are based on the theoretical resource [13].
- Seasonal changes in river width could not be captured as intended with satellite imagery, and as such the scope of this database is limited to one satellite imagery-derived width measurement. This assumption is expected to create an over-estimation of HK energy in the final product.
- The depth and slope will not be updated in the new dataset beyond what was produced in the regionalization method by Jenkinson and Bomhof [14]. Consequently, deep constrictions and sudden increases in riverbed slope, which are indicative of favorable HK energy conditions, are not captured in this dataset.

2 Data and Information Sources

2.1 Discharge Information

The previous hydrokinetic database developed by Jenkinson and Bomhof [14] (the 2014NRC database) included streamflow estimates in a 17-point flow duration curve (FDC), a cumulative probability distribution of the discharge at a river section. The database was presented as polylines with each line segment containing the 17 discharges associated with the 17 flow exceedance probabilities which are presented in Table 1. The polylines conformed to the structure of the archived Atlas of Canada 1,000,000 National Frameworks Data [17] which are grouped by major watershed, as illustrated in Figure 1.

The flow estimated were derived from a regionalization approach, namely multiple linear regression coupled with canonical correlation analysis (MLR-CCA), which utilized measured flows at Water Survey of Canada (WSC) gauge stations to estimate flows at ungauged locations based on watershed similarities. These watershed similarities included land cover, soil characteristics, surficial geology, and climate data. Estimates of depth, width, velocity, and power were also presented as attributes in the polyline database across the 17 flow exceedance probabilities.

Table 1: 17-point FDC exceedance probability index

FDC Index	Probability of Exceedance [%]
1	0.01
2	0.1
3	0.5
4	1
5	5
6	10
7	20
8	30
9	40
10	50
11	60
12	70
13	80
14	90
15	95
16	99
17	99.9

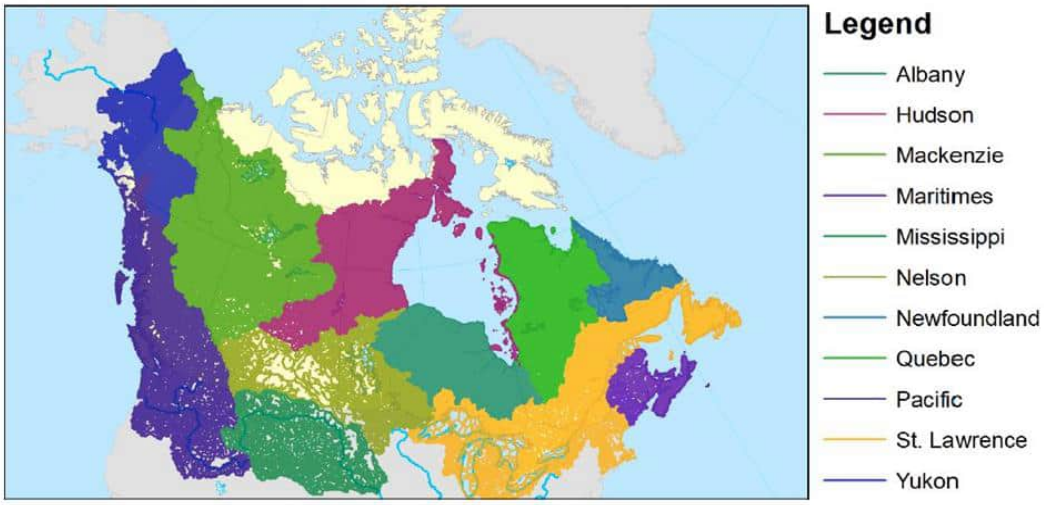

Figure 1: Major watersheds for which width, depth, velocity, and hydrokinetic power estimates were computed for each reach in the 2014NRC database. Figure taken from Bomhof [18].

As described by Jenkinson and Bomhof [14], regionalization parameters were calibrated and optimized, in part, to minimize error between predicted flows (from the MLR-CCA analysis) and measured flows from WSC gauges. Flow predictions were also augmented with measured flows where WSC gauges existed. In addition to predicted flow values, Jenkinson and Bomhof [14] reported lower and upper flow estimates (based on the 95% prediction interval) as well as the confidence interval for each of the 17 flow exceedances at each line segment. Readers are directed to relevant project literature for the 2014NRC database ([14], [18], [19]) for additional detail pertaining to flow estimates and uncertainty.

In 2022, the Department of Civil Engineering and Trottier Institute for Sustainability in Engineering and Design at McGill University developed a dataset of river discharges of Canadian rivers [20]. The dataset is available in NetCDF format with daily discharge estimates from 1979 to 2016 driven by the regional climate model Global Environmental Model (GEM) developed by Environment and Climate Change Canada. The GEM hydrological data is discretized on a 50km grid, and this was downscaled to 5km resolution using a modified version of the draining routing scheme WATROUTE [20], [21]. Teufel and Sushama [20] concluded that the 5km discharge estimates compared fairly well with the flow estimates generated by Jenkinson and Bomhof [14].

To convert runoff calculated from GEM to streamflow, the routing scheme employed a modified version of Manning's equation, an assumed channel cross-sectional shape, flow directions, river slopes, and river lengths from the HydroSHEDS database. Daily streamflow estimates are available for the entirety of Canada, unlike the 2014NRC database which excluded streamflow estimates for the Arctic and some areas of southern Saskatchewan, as illustrated in Figure 2.

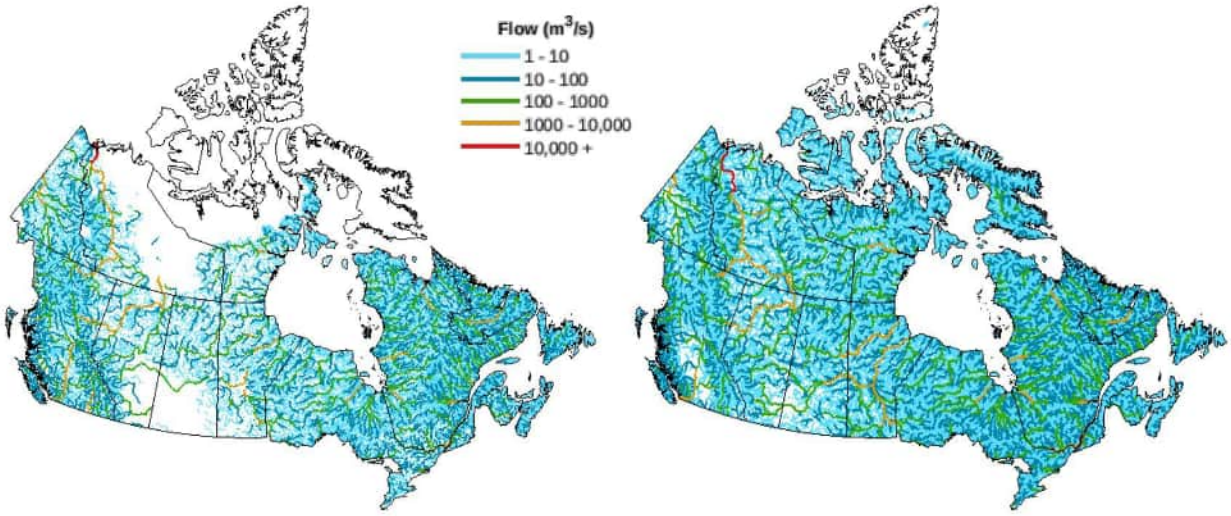

Figure 2: Mean annual streamflow from (left) Bomhof and Jenkinson [14] and (right) Tuefel and Sushama [20]. Figure taken from Tuefel and Sushama [20].

2.2 River Depth Information

Estimates of river depth were not expected to be improved beyond the work completed by Jenkinson and Bomhof [14] illustrated in Figure 3, due to the low availability of required data across the entirety of Canada and the limitations of the methods currently available [10]. As such, the regionalized depth estimates provided in the 2014NRC database [14] were adopted for the new database.

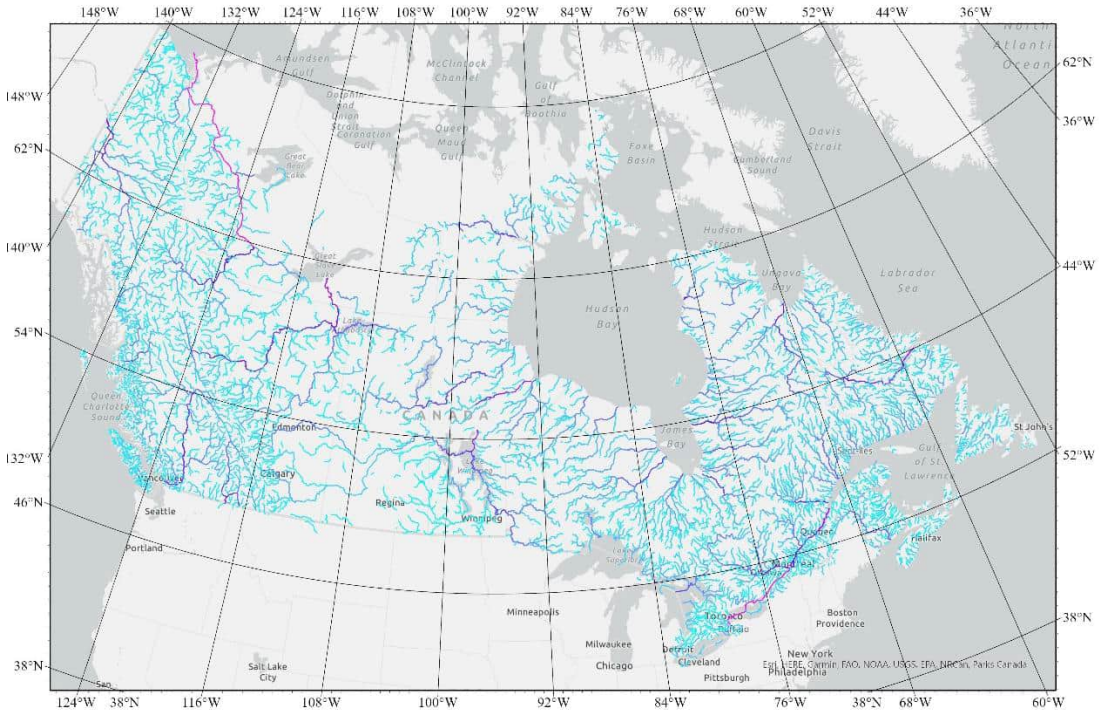

Figure 3: River depth estimates at mean annual flow from Jenkinson and Bomhof [14].

Jenkinson and Bomhof [14] developed and applied at-a-station and downstream hydraulic geometry relationships to estimate channel geometry for the 2014NRC database. At-a-station hydraulic geometry relationships describe the variation in channel geometry (i.e. width and depth) in response to different flow conditions at a specific cross-section, whereas downstream hydraulic geometry relationships describe variation in channel geometry along the length of the river for a specific flow condition [22], [23]. Downstream hydraulic geometry relationships are often defined based on channel forming flow [23]. The channel-forming flow is the flow that is theorized to transport the most sediment [24], [25] (outside of extreme events that are infrequent), thus forming the shape of the channel. The bankfull flow condition is commonly adopted as the channel-forming flow and generally corresponds to a reoccurrence interval of 1 to 2.5 years [23], [25]. Both at-a-station and downstream hydraulic geometry relationships conform to the following structure [22].

$$w = aQ^b \quad (2\text{-}1)$$
$$d = cQ^f \quad (2\text{-}2)$$
$$v = kQ^m \quad (2\text{-}3)$$

where w is width and d is depth. In addition, the continuity equation needs to be respected:

$$Q = wdv = aQ^b \times cQ^f \times kQ^m \quad (2\text{-}4)$$

thus:

$$b + f + m = 1 \quad (2\text{-}5)$$
$$a \times c \times k = 1 \quad (2\text{-}6)$$

Jenkinson and Bomhof [14] developed at-a-station hydraulic geometry relationships (ASHG) using data from the Water Survey of Canada Measurement Database (WSC-MD), which contains measurements of depth, width, and cross-sectional area recorded at gauge stations during multiple flow conditions. From the derived ASHG relationships, Jenkinson and Bomhof [14] estimated the width, depth, and area for each gauge station and at each flow corresponding with the 17 points on the FDC. In addition, they derived downstream hydraulic geometry (DHG) relationships for each of the 17 flow exceedance conditions. These DHG relationships were then used to estimate width, depth, and cross-sectional area at ungauged locations based on the flow of a particular flow exceedance.

Jenkinson and Bomhof [14] applied a Monte Carlo approach to quantify and express uncertainty of their channel geometry estimates. In summary, 1000 flows were computed for each flow condition (i.e., each of the 17 flows of the FDC) for each river segment in accordance with the statistical regression analysis (MLR-CCA) described in Section 2.1 as a foundation for Monte Carlo analysis. Jenkinson and Bomhof [14] used the hydraulic geometry relationships that they developed to estimate channel widths and depths for each sample flow. Ultimately, they computed 1000 widths and depths for each flow frequency for each river segment in their database as a basis to quantify uncertainty (presented as the 95% prediction interval for width and depth for each flow frequency for each river segment).

Readers are directed to relevant project literature for the 2014NRC database ([14], [18], [19]) for additional details pertaining to depth estimates and uncertainty.

2.3 River Width Information

2.3.1 National Hydro Network

The National Hydro Network (NHN) [26] is a database of inland surface water features including polygons (lakes, rivers, reservoirs, drainage basins, etc.), lines (river centerlines, drainage routes, etc.), and points

(hydro obstacles, junctions, etc.). The database was developed from multiple datasets with a maximum 1:50,000 scale. The datasets used to generate the NHN are not identified in the metadata; thus, the dates of the imagery used to develop the water polygons is not known. As such, the applicability of the NHN was limited because the flow stages associated with water polygons (and, by extension, derived information such as channel widths) are unknown. Additionally, the water polygons in the NHN may be out-of-date in areas where waterbodies have migrated since the development of the database. Such migration from the original position of the waterbodies in the NHN was observed during the work outlined in this report. The NHN centerlines have unique IDs that can improve data transferability to other national spatially referenced datasets, so the NHN centerlines were used as a skeleton to map river parameter attributes (see Section 3.2).

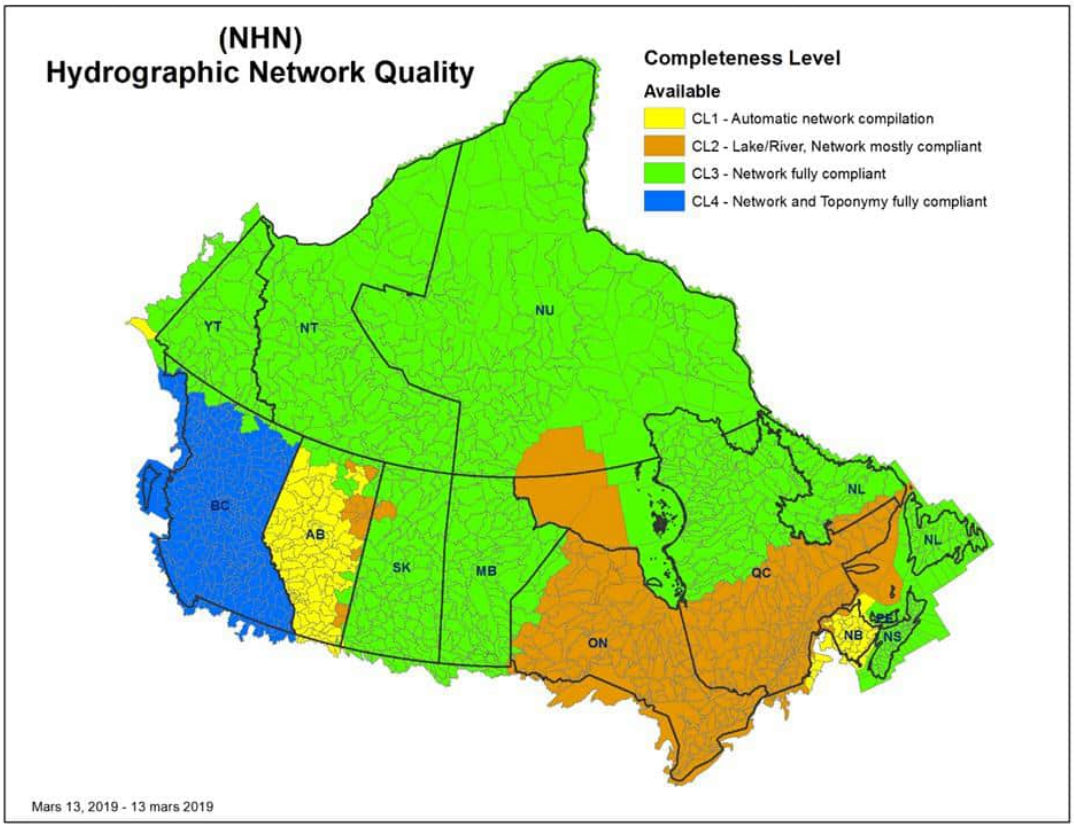

Figure 4: NHN areas [26].

2.3.2 Remotely Sensed Imagery

Sentinel-2 Multispectral Instrument (S2MSI) [27] Level 2A imagery was used to extract river widths directly. This particular imagery product was selected because the imagery is atmospherically corrected and orthorectified, limiting the amount of preprocessing required to interpret land and water features. The European Space Agency began systematically generating Level-2A products in December of 2018 [28]. Therefore, imagery-derived width analyses were based only on images collected during or after the year 2019. Additionally, only satellite imagery from ice-free months (May, June, July, August, September, and October) was used to derive estimates of river width, as discerning ice pixels from snow or land pixels is not yet possible. The use of spectral-based imagery did also require that the imagery was relatively cloud free. Cloud cover and snow/ice information was available in the metadata and locations of clouds were available in the S2MSI Scene Classification Layer (SCL). As such, the images were able to be filtered by a certain percentage of total allowable cloud or snow/ice in the image, and a mask was applied to exclude cloud, cloud shadow, and snow/ice areas.

Radar-based imagery (e.g., Sentinel-1 imagery [29]), although cloud free and not influenced by shadows, cannot extract water as accurately when compared to S2MSI spectral-based imagery [30]. Spectral-based imagery is able to capitalize on the range of absorption of light wavelengths that is different between water and non-water objects [30], [31]. Figure 5 illustrates the difference in absorption of light in different wavelengths between water and non-water objects. Radar-based imagery does not have this advantage. Radar imagery can also be heavily distorted in high relief areas by the topographical correction process [30]. This can have the consequence of losing almost all water pixels in canyons.

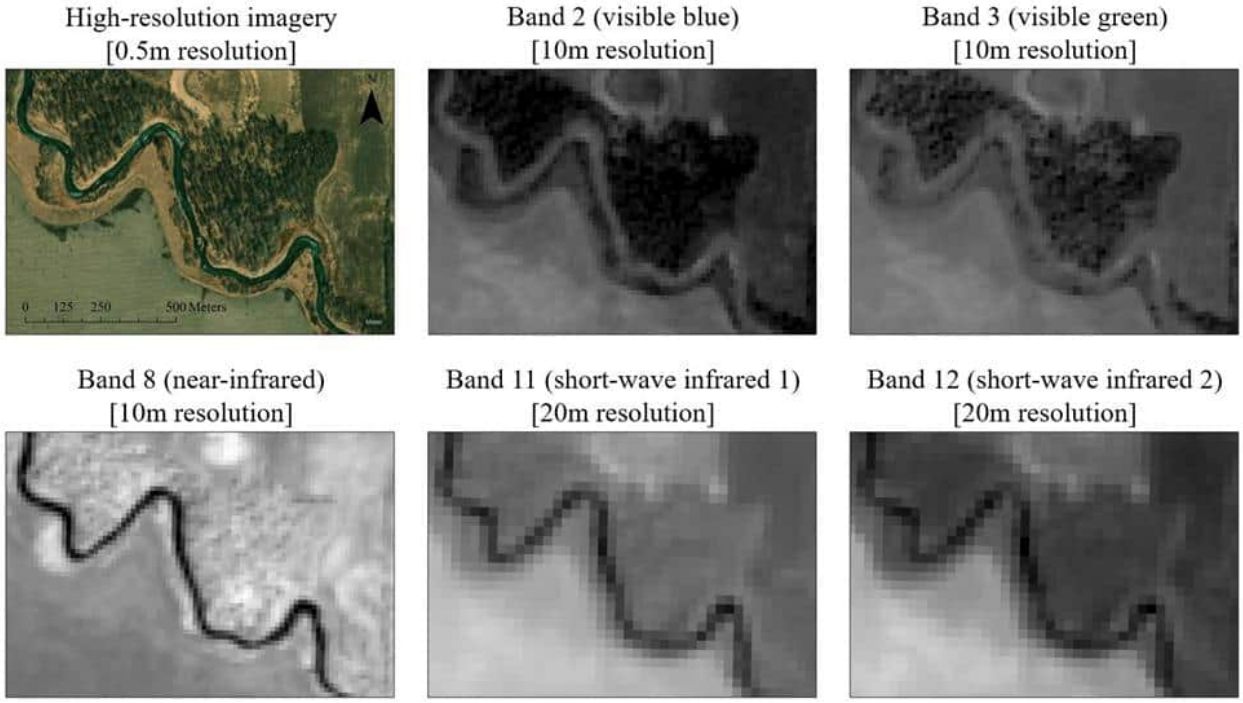

Figure 5: High-resolution red, green, blue false colour imagery (top-left image) compared to Sentinel-2 spectral-based imagery.

S2MSI consists of two satellites (S2A and S2B). Combined, the mission has a repeat cycle of 5 days [32]. The capture date of the imagery is available in the metadata, so a measured or approximated flow can be associated with the channel widths extracted from the imagery. The imagery can also be filtered by date to create a mosaic of imagery in Google Earth Engine. S2MSI products can be accessed through Copernicus Open Access Hub, through the Living Atlas in ArcGIS Pro, through Google Earth Engine, or by any other service that has access to the S2MSI level 2A imagery catalogue. Depending on the specific band, S2MSI imagery has a spatial resolution ranging from 10m to 60m [33]. The finer resolution bands provide an advantage for mapping surface water features in detail compared to lower resolution imagery, such as the Moderate Resolution Imaging Spectroradiometer (MODIS) [34], [35]. The resolution and wavelength of S2MSI imagery bands is presented in Table 2. The resolution of the imagery does limit the size of waterbodies that can be detected from satellite imagery as well as limits the ability to detect small- to medium-sized waterbody seasonal shoreline changes.

Table 2: S2/MSI imagery resolutions and wavelengths [27]

Band	Resolution [m]	Central wavelength [µm]	Description
1	60	0.443	Coastal & aerosol
2	10	0.490	Blue
3	10	0.560	Green
4	10	0.665	Red
5	20	0.705	Visible & NIR
6	20	0.740	Visible & NIR
7	20	0.783	Visible & NIR
8	10	0.842	Visible & NIR
8a	20	0.865	Visible & NIR
9	60	0.940	SWIR
10	60	1.375	SWIR
11	20	1.610	SWIR
12	20	2.190	SWIR

3 Methods

3.1 General Approach

To calculate the riverine HK power, the kinetic power equation, equation (1-1), and the kinetic power density equation, equation (3-1), were used.

$$\frac{P_K}{A} = \frac{1}{2}\rho v^3 \tag{3-1}$$

Calculating HK power (P_K) required water density (ρ), river cross-sectional area (A), and velocity as inputs (v). Velocity was calculated using continuity (equation (3-2)) with flow (Q), river width (w), and river depth (d).

$$v = \frac{Q}{A} = \frac{Q}{w \times d} \tag{3-2}$$

A velocity associated with each flow exceedance on the 17-point FDC (flow exceedance percentiles illustrated in Table 1) was calculated from continuity to create velocity duration curves (VDC). Then, a power associated with each flow exceedance and velocity on the VDC was calculated using the kinetic power equation, and a power duration curve (PDC) was then developed for each point in the database. Using each PDC, the annual expected power (AEP) was calculated at each point using equation (3-3) below from the IEC [13] standards for river HK energy resource estimation:

$$AEP = N_h \sum_{i=1}^{N_B} P_i B_i \tag{3-3}$$

where N_h is the number of hours of turbine operation in a year, N_B is the number of points on the PDC, P_i is the theoretical power present at the point on the PDC, and B_i is the width on the PDC that the point represents as a decimal probability.

3.2 Database Structure

The NHN watercourse centerlines served as the framework for integrating flow, depth, and width information. Points were generated at specific intervals along the centerline, with intervals of either 100m, 200m, or 400m, depending on the river width at that particular section of the centerline. This is further described in Section 3.3.1. Points located in the vicinity of river confluences and other areas where two or more rivers come within

close proximity (1500m) to one another were removed from the database to facilitate accurate mapping of flow and depth values from the 2014NRC database developed by Jenkinson and Bomhof [14].

Methods employed to map flow and depth values from the 2014 database are described in Section 3.4. The resulting database (where channel widths were derived from the NHN database) was composed of 1,291,270 points (Figure 6); future iterations of the database may differ in size depending on the methods used to estimate channel width. The database is organized by major watershed, delineated by both the WSC and in the NHN database. There are eleven major watersheds included in the hydrographic data, and each is shown by a different colour in Figure 6.

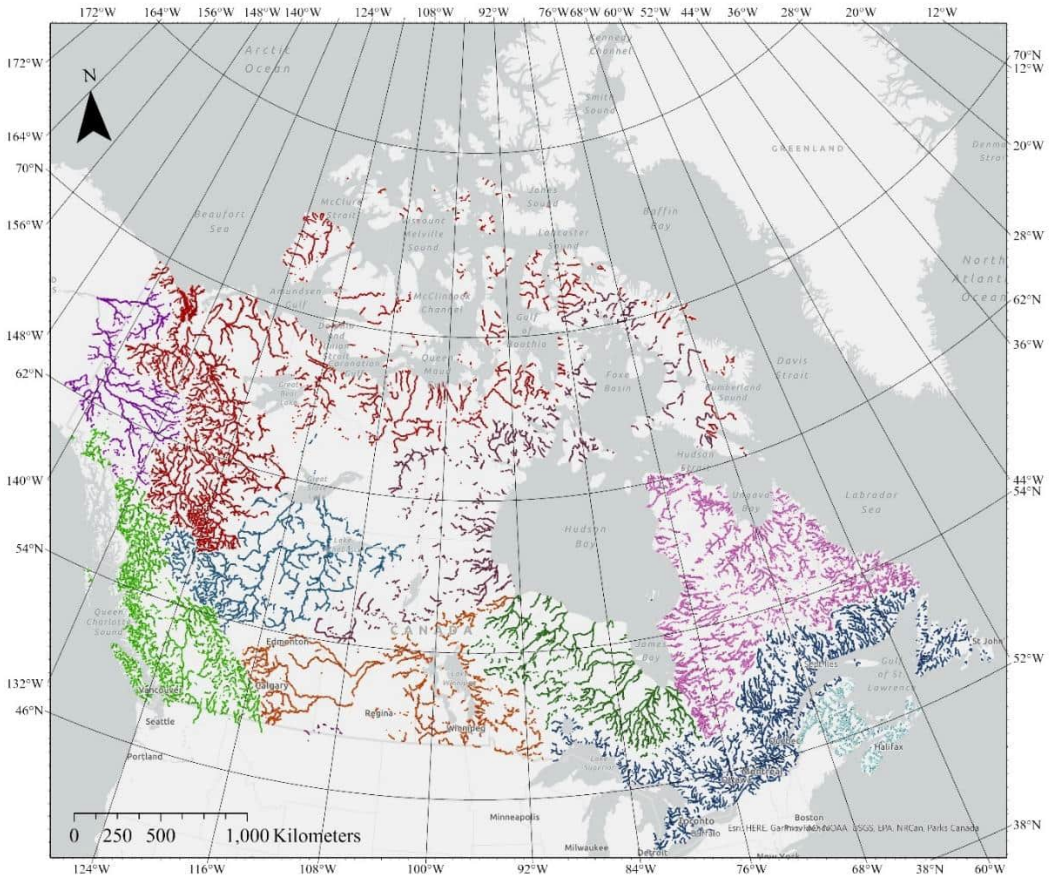

Figure 6: The newly developed hydrokinetic database in the form of points for which information regarding the flow was calculated.

The database was divided into two data files. The first file contains only the flow, depth, and width data (named NHN_##_Flow_Depth_Width) and includes information at flow splits. Where flow splits are present, the width values represent the width of the individual river branch (i.e., the primary branch or the secondary branch), and not the total channel width. The second file contains the flow, depth, width, velocity and power data (named NHN_##_Pwr). Flow splits are excluded from the second file to avoid erroneous and misleading velocity and power estimates in the vicinity of these features. The difference between the two files is illustrated in Figure 7. Further information on the flow split methodology is available in Section 3.3.1.

Figure 7: The difference between the two datasets around islands (i.e., flow splits). All velocity, power datapoints also have an associated flow, depth, and width datapoint.

3.3 Channel Width

3.3.1 River Widths from NHN

The NHN water polygons, in particular the river polygons, and associated centerlines were used to estimate river widths as a preliminary width value to be further refined using the satellite imagery methods. Several width estimation tools and methods were explored including RivWidth [36] the Geometric Attributes QGIS plugin [37] and tools available in ArcGIS Pro version 3.03. Ultimately, the width analysis was conducted using the ArcGIS tools which provided acceptable technical results as well as a user-friendly framework conducive to process automation. Widths were calculated at specified intervals along the river centerlines. Pre-processing of the NHN included:

1. Filtering by waterbody “definition” attribute equal to six.
2. Manual addition of rivers defined as reservoirs (“definition” = 5) or lakes (“definition” attribute = 4) in the dataset. For example, the Ottawa River was almost entirely defined as a reservoir in the database.
3. Clipping the centerlines to the river polygon extents.
4. Filtering the centerlines by “priority” attribute equal to one.
5. Removing centerlines that coincided with small rivers (which involved clipping the centerlines to a region defined by a 1500m buffer around line segments of the 2014NRC database where flows are expected to exceed $100m^3/s$ during the 99.9% flow exceedance condition – i.e., where at least the largest flows at a given location are expected to exceed $100m^3/s$).
6. Projecting both the centerlines and river polygons to North America Lambert Conformal Conic.
7. Smoothing the centerline with Simplify Line tool using 40m spacing and retain critical bends (using the Wang-Müller algorithm).

The river width calculation approach consisted of generating transects along the centerline, clipping those transects to the river polygon extent, and measuring the length of the clipped transects. ArcGIS Pro Version 3.03 was used to generate transects at equal spacing perpendicular to the NHN river centerlines. Because the ArcGIS Pro tool “Generate Transects Along Lines” was used to generate the perpendicular transects, and the tool requires the transect length as an input to generate the transects, a tiered approach was utilized as there was no a-priori knowledge of what the transect length needed to be to span the entire river cross section. As such, Model Builder was used to generate transects based on this criterion: the transects needed to intersect the banks twice as to not be too long that it intersected multiple waterbodies and not to short to not span the entire river cross section. The first tier in the processing was 100m long transects at 100m spacing. If the 100m transects did not meet the above criterion, a 200m long transect was generated at a spacing of 100m. If the 200m transect did not meet the criterion, a 500m long transect was generated at a spacing of 200m. The remaining three tiers were 1000m long transects with 400m spacing, 2000m long transects with 400m spacing, and 3000m transects with 400m spacing. The spacing increases with increasing transect length to reduce computational time in future processing steps and to limit space requirements where increased resolution is not likely to capture abrupt changes in river width.

The resulting transects were clipped to the NHN river polygon dataset, and the lengths of the transects were measured (w_{total}). Both NHN centerline information and the calculated width information were transferred to intersection points between the centerlines and the transects. These points generated at the intersection of transects and centerlines represent the structure of the final database (see Section 3.2). Additionally, the transect length on one side of the centerline was calculated (w_1) to calculate the width similarity (WS) with equation (3-4) below.

$$WS = 100 \times (1 - \frac{w_{total} - 2 \times w_1}{w_{total}}) \quad (3\text{-}4)$$

Braided channels, islands, sand bars, and other riverine obstacles that induce flow splits were flagged using the NHN Flow_Split attribute equal to 2. Points that are not located at a flow split have the Flow_Split attribute equal to 1. In the vicinity of flow splits, the reported width values represent the width of the individual river branch (i.e., the width of the primary channel or secondary channel) and do not represent the total channel width. Points in the vicinity of flow splits were flagged to avoid misinterpretation of the data; the flow data reported in the vicinity of flow splits represent the total flow moving through the primary and secondary channel(s), whereas the width data reported in the vicinity of flow splits represents the width of the individual channel only. Velocity and power estimates were not reported in the vicinity of flow splits; it is challenging to estimate the proportion of flow moving through individual branches of a multi-channel system without detailed, site-specific investigation. Points located within approximately 250m of island features that have a length exceeding 100m (i.e., an NHN island polygon coinciding with a flow splits) were identified and flagged.

The resulting database attributes are:

- **T_ID**: A unique ID for each generated transect. This was used to join imagery-derived widths to the existing database.
- **Total_Width**: The NHN-derived width representing only the primary channel (i.e., priority 1 river centerlines in the NHN dataset) at flow splits.
- **Width1**: The width on one side of the centerline to the bank.
- **Width_Similarity**: A comparison of the widths on either side of the centerline. This attribute can be used to identify centerlines that are not centered between the banks or to identify bad transects.
- **Flow_Split**: Identifies locations at or near channel braids, islands, sand bars, and other obstacles that create a division of the estimated flow value.

3.3.2 Satellite Image Surface Water Extraction

Surface water features were extracted from imagery in an effort to supplement and improve width estimates. The widths derived from the NHN could not be associated with a date or flow condition, and the NHN polygons poorly represented the actual channel geometry in some regions. The Automated Water Extraction Index, No Shadow (AWEI_NSH) spectral index method was chosen to extract surface water from S2MSI satellite imagery because the method is accurate at detecting surface water and differentiating water from non-water objects [30]. Some non-water and water objects, such as urban built-up, wet sand, and shallow vegetation are difficult to classify accurately; however, AWEI_NSH is comparatively more accurate than other common spectral index methods at classifying these objects [30]. Additionally, AWEI_NSH has a relatively stable threshold [30], [31], meaning that the process is less sensitive to threshold selection and is more conducive to broad application across multiple images. The AWEI_NSH index is presented in equation (3-5).

$$AWEI_{NSH} = 4 \times (\rho_{green} - \rho_{SWIR1}) - 0.25 \times \rho_{NIR} - 2.75 \times \rho_{SWIR2} \quad (3\text{-}5)$$

where ρ_{blue} is the blue band with bandwidth 0.439 to 0.522 µm (band 2 in S2MSI imagery), ρ_{green} is the green band with bandwidth 0.538 to 0.583 µm (band 3 in S2MSI imagery), ρ_{NIR} is the near infrared band with

bandwidth 0.837 to 0.881 µm (band 8 in S2MSI imagery), ρ_{SWIR1} is the shortwave infrared band with bandwidth 1.539 to 1.682 µm (band 11 in S2MSI imagery), and ρ_{SWIR2} is the shortwave infrared band with bandwidth 2.078 to 2.320 µm (band 3 in S2MSI imagery). Unlike other common index methods that are normalized, such as the Normalized Difference Water Index (NDWI) or Modified Normalized Difference Water Index (MNDWI), the AWEI_NSH is not a normalized index. As such, digital numbers (DN) of the imagery pixels need to be converted to reflectance values based on equation (3-6) [38].

$$DN = 10{,}000 \times Reflectance \tag{3-6}$$

Google Earth Engine (GEE) was used for cloud-based imagery processing. The advantages of cloud-based image processing were the ease of calling and filtering the imagery, the ease and speed of processing the imagery, the ability to mosaic the entire S2MSI level 2A catalogue, and the computational storage saved by downloading only the final AWEI_NSH indexed image rather than downloading the six required bands of imagery separately. The main disadvantage of using GEE is that pre-constructed area of interest (AOI) polygons cannot be imported to specify the processing extent without a Google Cloud account behind a paywall. Such AOI polygons need to be manually drawn without access to a Google Cloud account. The script used to filter, mask, process, and extract the imagery using Google Earth Engine is available in Appendix A. Firstly, the desired imagery was called from the Sentinel-2 Copernicus Level 2A catalogue. Then, a mask was applied based on the SCL S2MSI layer to remove cloud and cloud shadow areas. The imagery was filtered by date, cloud cover (less than 20%), and presence of snow/ice (less than 0.1%). The date filter was set to select images by month and year. The first image available in an area that met the filter criteria was called from the S2MSI catalogue. The imagery was mosaicked for processing and download. After pre-processing and mosaicking, the AWEI_NSH method was used to create an indexed image and a threshold was applied to classify the image into water and non-water pixels. The resulting classified image, shown in Figure 8 for major WS1, was exported from GEE to Google Drive and was available for download to a local drive. Geometric white areas in Figure 8 indicate areas where sufficiently cloud-free images could not be identified from September 1, 2022 to September 30, 2022. Figure 9 presents a magnified view of the classified S2MSI mosaic for September 2022. The remaining processing steps – polygonising and selection of river polygons by intersection with NHN water polygons – were completed in ArcGIS Pro version 3.03. This process was completed for NHN major WS1, which includes New Brunswick, Nova Scotia, Prince Edward Island and part of Quebec near the Gaspé Peninsula. In total, 24 mosaics were extracted for years 2019 to 2022 and months May to October.

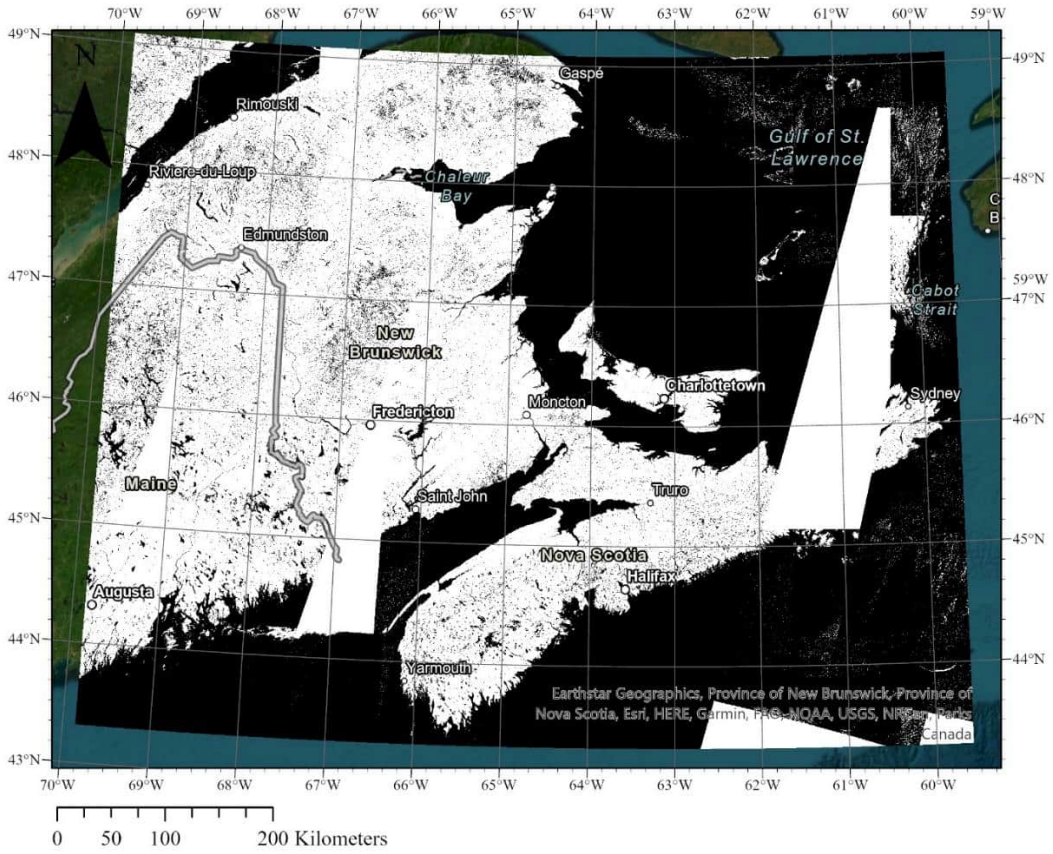

Figure 8: Water and non-water classified Sentinel-2 imagery mosaic for NHN WS1 for September 2022. Water features appear black and land features appear white. Geometric white areas indicate locations where sufficiently cloud-free images could not be identified.

A conservative threshold of -0.3 was applied across the entire mosaic to classify the pixels into water and non-water. However, through optimization, it was determined that a threshold range of -0.2 to 0 was most effective for accurately extracting water from S2MSI imagery with AWEI_SH, as it helped to reduce both commission errors (non-water objects classified as water) and omission errors (water objects classified as non-water) [30]. The optimal threshold is identified when the balance between commission errors and omission errors is achieved. Above this threshold, the omission error increases more than the commission error decreases. Conversely, below this threshold, the commission error increases more than the omission error decreases.

To further improve the accuracy of the final classified image and reduce commission errors, the NHN river polygons were utilized. Objects classified as water that do not intersect with the NHN river polygons were removed from the results, thereby minimizing the impact of commission errors.

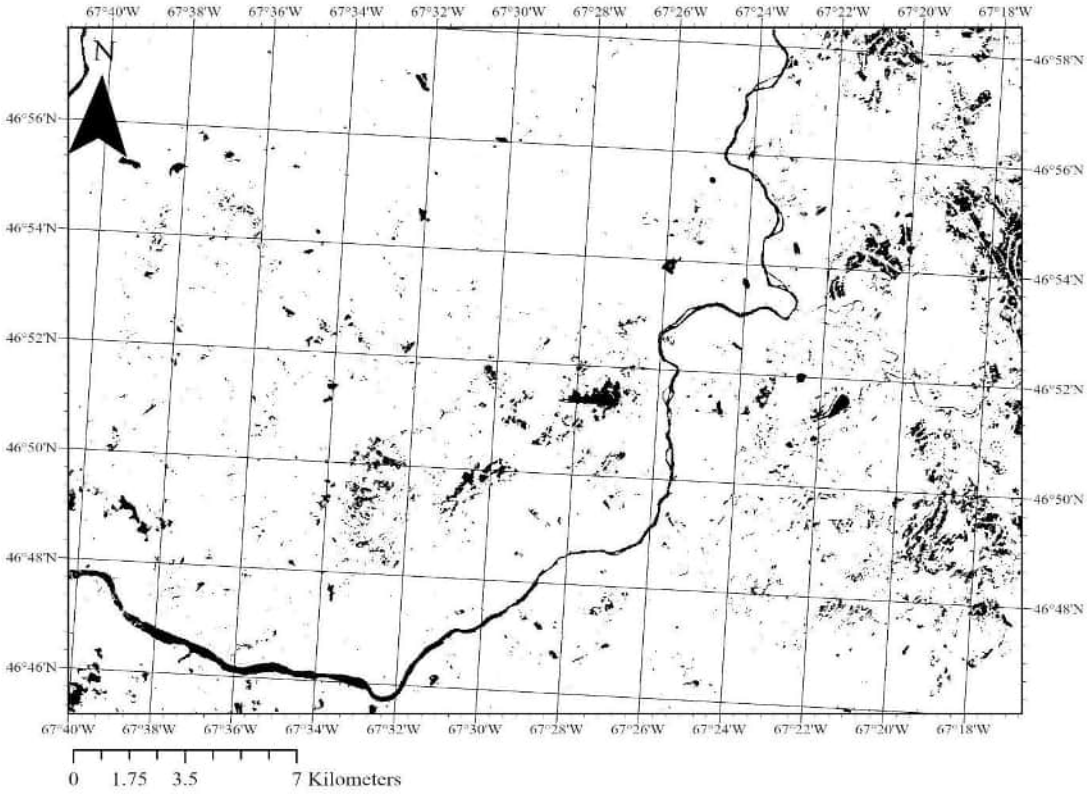

Figure 9: Water and non-water classified Sentinel-2 imagery of Tobique River, New Brunswick. Water features appear black and land features appear white.

3.3.3 River Width from Satellite Imagery

Estimating river widths from classified S2MSI imagery was only performed for points where the NHN-derived widths were greater than 40m in WS1. Because the resolution of the classified imagery is 20m, rivers smaller than 40m were not expected to be better represented with S2MSI imagery compared to the NHN polygons. The points generated from the NHN centerlines were used to store the imagery-derived width attributes.

Transects were generated along the NHN centerlines using the same process as described in Section 3.3.1, but the banks derived from the classified imagery were used in place of the NHN water polygon banks. The transects were clipped to the imagery-derived polygons and the lengths of the transects were measured. This width information was transferred to the database points by utilizing the common attribute, T_ID, which allowed imagery derived widths to be mapped onto the database points, even where there was some misalignment between imagery derived water features and NHN water features owing to channel migration.

This process was repeated for 24 classified S2MSI mosaics for major WS1 to extract river width information from years 2019, 2020, 2021, and 2022 and, in those years, months May, June, July, August, September, and October. As a quality check, imagery-derived widths that differed from the NHN-derived widths at the same location by ±50% were discarded. The widths were then averaged by month. The resulting attributes were multi-year averaged widths for May, June, July, August, September, and October.

3.3.4 River Width and Flow Exceedances

An analysis was performed using available gauge data in an attempt to develop width duration curves (WDCs) to represent the relationship between imagery-derived month-representative widths and average monthly flows. In short, the flow exceedance data from gauge stations was spatially joined to month-representative widths using the NHN subsub-drainage basin polygons. It was expected that a negative relationship would be

developed between width and flow exceedance, as river width generally increases as flow increases (i.e., as flow exceedance decreases).

However, contrary to the initial expectation, the analysis revealed an approximate 50/50 split between negative and positive slope for this relationship across the database in NHN major WS1. As such, the imagery-based widths will not be presented in a WDC format (i.e., a width estimate for each flow exceedance in Table 1), and rather the mean, maximum, and minimum widths derived from imagery will be used to calculate the mean, minimum, and maximum hydrokinetic power estimates, respectively. Further information on this analysis and findings are available in Section A.2.

3.4 Flow Duration Curves and Channel Depth

Flow and depth data were adopted from the 2014NRC database developed by Jenkinson and Bomhof [14] for all regions excluding the Arctic; the 2014NRC database did not include the Arctic. Using the Atlas of Canada Hydrology – Drainage Network as a framework, Jenkinson and Bomhof [14] estimated a 17-point flow duration curve and 17-point depth duration curve for every river segment in the Atlas of Canada River Network.

Given that there are no identification keys or schematics to facilitate joining or spatial relationships between the archived Atlas of Canada River Network and the modern NHN framework, the ArcGIS's Spatial Join tool [39] was employed to map flow and depth values from the 2014 database (discretized as line segments) onto the new database (discretized as points). A "closest" match option was specified, meaning that flow and depth values from the closest line segment in the 2014 database were mapped onto each point in the new database. A maximum search radius of 1500m was specified to alleviate the possibility of erroneous mapping.

As specified in Section 3.2, points located in the vicinity of river confluences and other areas where two or more rivers come within close proximity (1500m) to one another were removed from the database to further alleviate the possibility of erroneous mapping. The mapping procedure is illustrated in Figure 10.

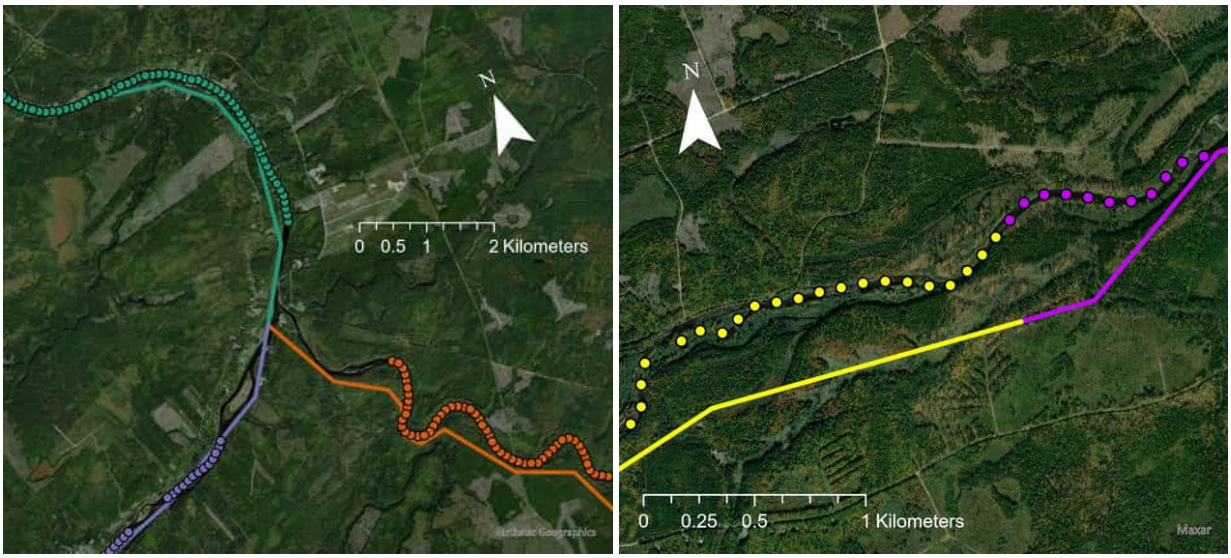

Figure 10. Example of the mapping procedure employed to map flow and depth values from the 2014NRC database (lines) onto the updated database (points) using the ArcGIS Spatial Join tool. The mapping procedure is shown in the vicinity of a confluence (left) and along a river channel (right). Common colours indicate mapped pairs (i.e., values from the green line were mapped onto the green points).

3.5 Velocity and Power Duration Curves and Hydrokinetic Energy

For all datapoints not associated with a flow split, the cross-sectional velocity was calculated using equation (3-2), which assumes a rectangular channel shape. A velocity for each flow exceedance in Table 1 was calculated from each flow and depth associated with the flow exceedances and an NHN-derived width.

For WS1, where imagery-derived widths were available, upper, lower, and mean velocities were calculated for each flow exceedance based on the minimum, maximum, and mean widths extracted from imagery, respectively. The following are the attributes related to velocity in the database:

- **Nvel**: Velocity calculated from NHN-derived width
- **IVel**: Velocity calculated from mean imagery-derived width
- **IMinVel**: Velocity calculated from maximum imagery-derived width
- **IMaxVel**: Velocity calculated from minimum imagery-derived width

From the velocity data, a hydrokinetic power value associated with each flow exceedance was calculated using equation (1-1). For WS1, upper, lower, and mean power estimates were calculated for each flow exceedance based on the minimum, maximum, and mean imagery-derived widths.

For all other watersheds, only one power value is available for each flow exceedance. This calculation facilitated a PDC from which AEP could be calculated for each river location using equation (3-3). The following are the attributes related to power and AEP in the database:

- **NPwr**: Power calculated from NHN-derived width
- **IPwr**: Power calculated from mean imagery-derived width
- **IMinPwr**: Power calculated from maximum imagery-derived width
- **IMaxPwr**: Power calculated from minimum imagery-derived width
- **N_AEP**: AEP calculated from NHN-derived width
- **I_MEAN_AEP**: AEP calculated from mean imagery-derived width
- **I_MIN_AEP**: Power calculated from maximum imagery-derived width
- **I_MAX_AEP**: Power calculated from minimum imagery-derived width
- **AEP**: This value will default to I_MEAN_AEP. Where I_MEAN_AEP is not available, this value will be N_AEP.

4 Results

4.1 Estimated River Width

4.1.1 NHN-Derived River Width

River widths were successfully extracted from the NHN waterbody polygons everywhere in Canada, as shown in Figure 11. The database point spacing increased with increasing river width based on the transect generation procedure. The specified point spacing (100m spacing for river widths less than 500m and 400m spacing for river widths greater than 1000m) appeared to capture width constrictions reasonably well. The NHN centerlines attributes are also linked to the database points for ease of data transferability between national datasets.

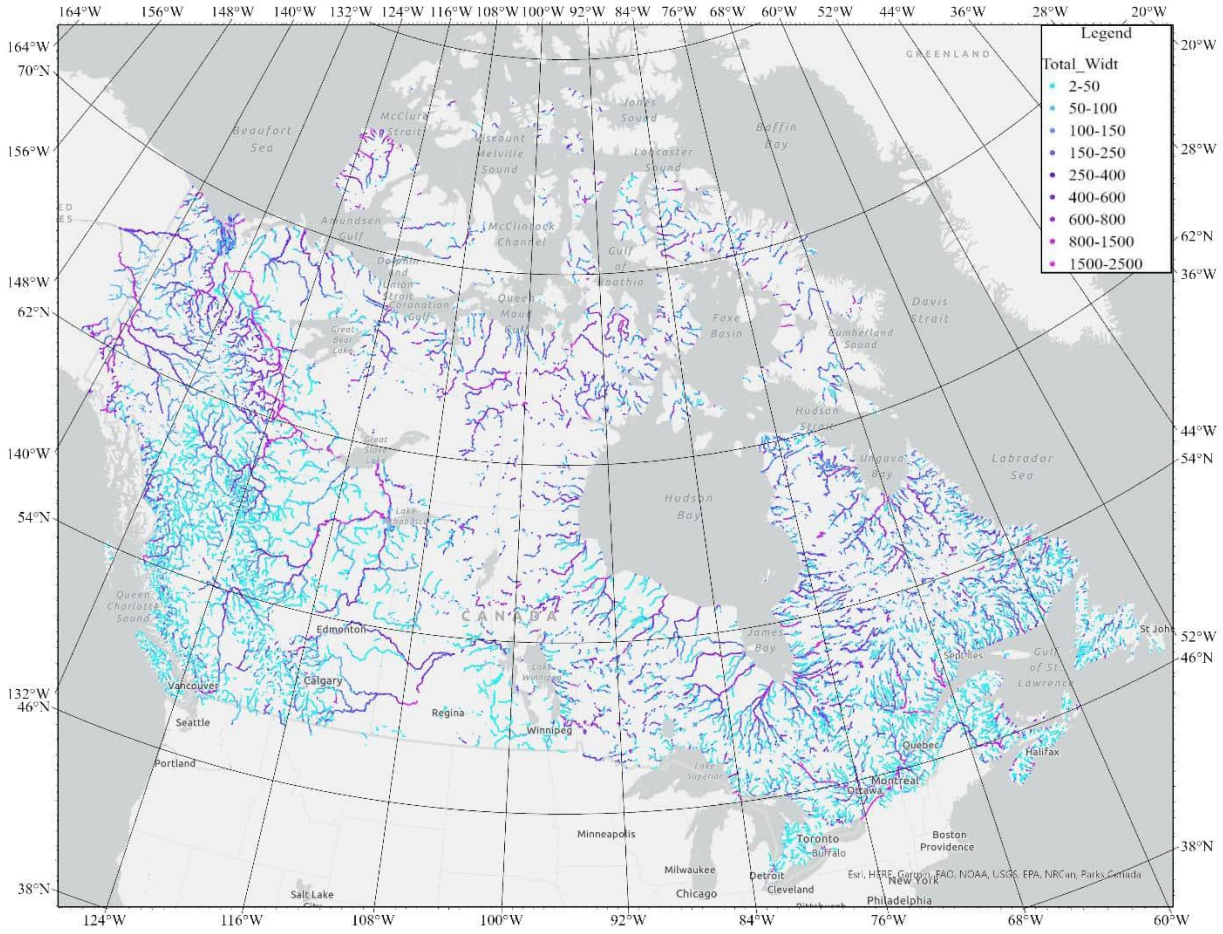

Figure 11: NHN-derived river widths in meters.

In some cases, rivers with complex riverbanks posed challenges for generating transects at certain locations. These challenges arose when the transects would intersect with the banks more than two times, regardless of the transect length. However, it was observed that these situations were rare and usually only one or two transects in the series of transects would be discarded; thus, continuity of the point database was minimally disrupted by these cases.

Points located directly at, upstream, and downstream of flow splits, such as islands, were flagged using the Flow_Split attribute equal to two (shown in Figure 12 as blue points rather than pink) as described in Section

20. Figure 12 illustrates the transects that were clipped to the water polygon extents in order to calculate river width as well as the database points at the intersection of each transect and the NHN centerline.

Figure 12: NHN-derived transects and width points on the Spanish River near Massey, Ontario.

4.1.2 Imagery-Derived River Width

A spatial comparison of the river width measurements from the 2014NRC database to the NHN-derived widths and imagery-derived widths is illustrated in Figure 13. The spatial trend of the imagery-derived widths compared to the NHN-derived widths was visually similar. The 2014NRC database tended to underestimate river width, particularly for rivers wider than 500m; thus, HK power values calculated in the 2014NRC database are expected to overestimate the actual HK power.

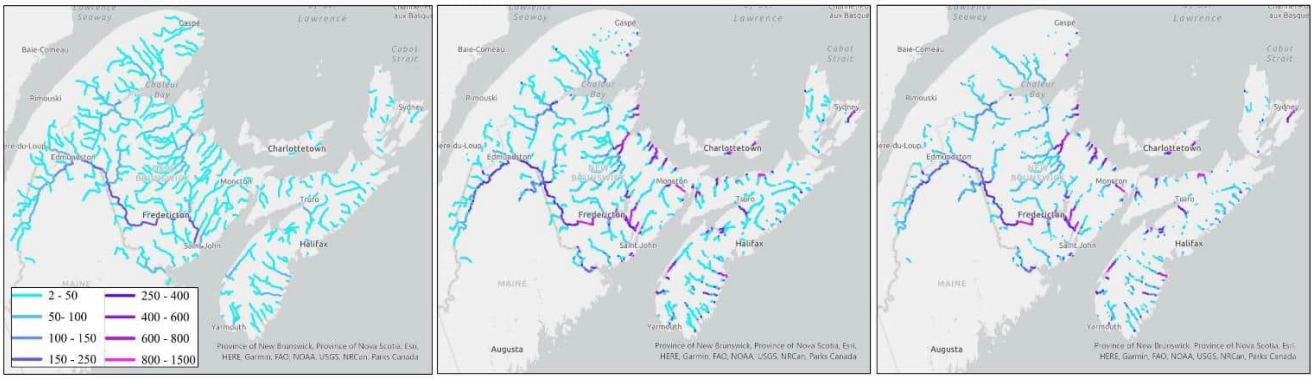

Figure 13: (Left) Widths generated in the previous HK assessment, (middle) widths extracted from the NHN polygons, and (right) widths extracted from satellite imagery in major WS1.

The number of width measurement attributes for each datapoint were dependent on the viable S2MSI imagery from years 2019 through 2022 and months May through October. Even with a 5 day repeat cycle, collecting

near-cloud-free imagery for each location for each month was not possible. The top left map of Figure 14 illustrates how many width measurements were collected at each of the datapoints in major WS1 out of the possible 24 measurements from years 2019 to 2022 and months May to October.

There was a trend apparent that larger rivers were more likely to produce datapoints with a higher number of width measurements. Smaller rivers were more likely to be missing width measurements because the resolution of the S2MSI imagery caused non-continuous water polygons. Additionally, specific areas in the watershed were more likely to be cloud covered. For example, not many S2MSI images met the cloud cover criteria on the west side of Cape Breton Island, near Edmundston, New Brunswick, and near Saint John, New Brunswick.

Furthermore, width points were removed from the dataset if the measurement was ±50% different from the NHN-derived width measurement because the difference was likely either caused by a cloud or cloud shadow that was not able to be removed in pre-processing or caused by an anomaly event, such as flooding. A flood takes place when the banks of the river are overtopped, which is when the bankfull flow condition, with a theorized return period of 1.5 to 2 years, is exceeded [40]. Images recorded during flood conditions could potentially skew the mean monthly width estimation to be larger than the true mean width. Additionally, these short-duration extreme events are not of interest to HK energy developers, who are interested in knowing the HK resource present in statistically frequent seasonal flow conditions.

Each width measurement based on a specific month was averaged, resulting in six mean month-based width measurements for each datapoint, corresponding to the months from May to October. The purpose of using the mean of the month-based width measurements was to increase the confidence in the width measurement for a typical month. For example, averaging the width measurements collected from May 2019, May 2020, May 2021, and May 2022 was expected to improve the confidence in representing a typical “May” width. The number of mean month-based widths available for each datapoint out of the total six is presented in the bottom map in Figure 14.

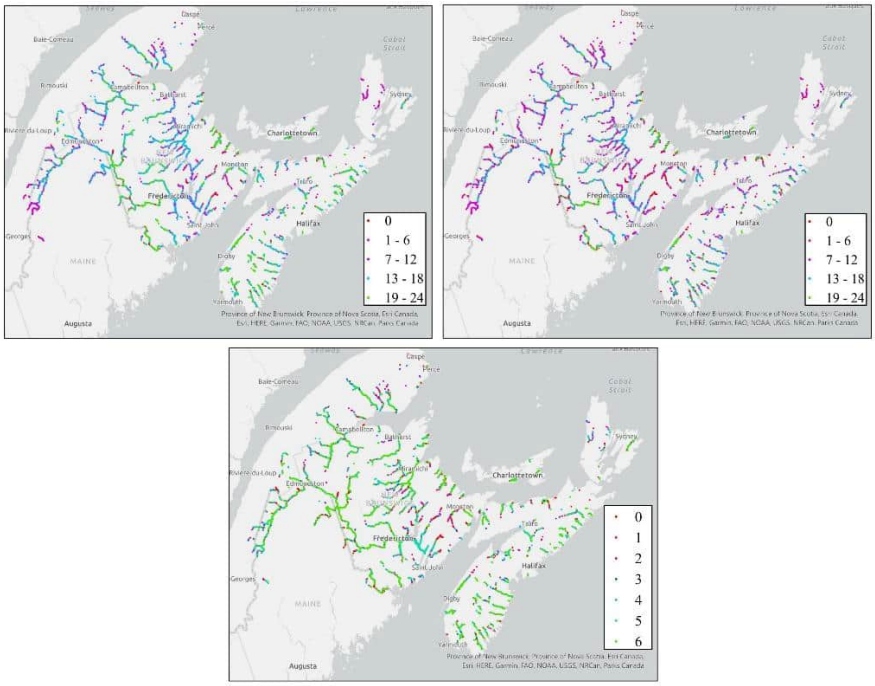

Figure 14: Imagery-derived width dataset completeness. (Top left) Width measurements at each database point out of the 24 possible month-based measurements. (Top right) Width measurements at each database point after filtering

measurements within ±50% of the NHN-based width measurement. (Bottom) Month-averaged width measurements available at each database point out of the six possible month-averaged measurements.

4.1.3 Comparison of Width Estimation Methods

A comparison analysis was performed between the mean month-averaged imagery-derived widths, the NHN-derived widths, and the widths from the 2014NRC database. The three estimates were compared against river polygons that were manually delineated from high resolution (i.e., pixel size 50cm X 50cm) satellite imagery in four locations: Red River, Manitoba; Fraser River, British Columbia; Riviere Rouge, Quebec; and Ottawa River, Ontario. Imagery-derived widths were generated for these four locations for the purpose of error analysis between the NHN-derived widths, the imagery-derived widths, and the NRC2014 widths. The manually delineated polygons were assumed to contain negligible error.

The number of width points (river cross-sections) compared is presented in Table 3. The statistical metrics to quantify the success of each width estimation method included the mean absolute error (MAE), the mean absolute percent error (MAPE), the root mean squared error (RMSE), and the percent error of the mean (PEM).

$$MAE = \frac{\sum_{i=1}^{N} |w_i - \hat{w}_i|}{N} \tag{4-1}$$

$$MAPE = \frac{1}{N} \sum_{i=1}^{N} \frac{|w_i - \hat{w}_i|}{v_i} \tag{4-2}$$

$$RMSE = \sqrt{\frac{\sum_{i=1}^{N} (w_i - \hat{w}_i)^2}{N}} \tag{4-3}$$

$$PEM = \frac{(\frac{\sum_{i=1}^{N} w_i}{N}) - (\frac{\sum_{i=1}^{N} \hat{w}_i}{N})}{(\frac{\sum_{i=1}^{N} \hat{w}_i}{N})} \tag{4-4}$$

where N is the number of datapoints or cross-sections, w_i is the actual width derived from the high-resolution imagery, and $\hat{w}_i$ is the estimated width from one of the three methods.

Both the NHN-derived widths and imagery-derived widths contained less error than the widths from the 2014NRC database, as illustrated in Table 3. Using the NHN polygons to estimate widths produced less error in smaller rivers (Red River and Riviere Rouge) than using imagery-derived water polygons. This is because the spatial resolution of the S2MSI imagery is too coarse to adequately define the banks of the Riviere Rouge at narrow sections. These two locations are also well represented by the NHN polygons and no noticeable channel migration has occurred since the creation of the NHN polygons.

Conversely, the larger rivers seem to be better represented by the imagery-derived polygons in the Fraser River and Ottawa River areas. This is because the NHN polygons represent only one flow condition. The flow condition that the NHN represents in these two locations did not happen to match with the high-resolution imagery and S2MSI imagery flow condition, whereas the high-resolution imagery and the S2MSI imagery represented the same flow condition. This was ensured by matching the dates of the high-resolution imagery and S2MSI imagery, or, in some cases, allowing only a few days of difference between the high-resolution imagery and the S2MSI imagery.

Table 3: Errors associated with river widths estimated using a regionalized hydraulic geometry approach and river widths estimated using a satellite imagery approach (S2MSI with AWEI_NSH)

Area of analysis (Number of cross-sections) *Mean actual width [m]*	**Method**	**Confidence interval**	**MAE [m]**	**MAPE [%]**	**RMSE [m]**	**PEM [%]**
Red River	2014NRC database	Lower	117.9	83.8	120.0	-82.2
		Middle	97.8	71.4	100.2	-62.0
(180)		Upper	60.1	50.6	63.0	-36.9
	S2MSI	-	10.0	7.5	12.3	-6.2
142.5	NHN	-	6.9	5.3	8.5	-3.9
Fraser River	2014NRC database	Lower	38.6	44.7	48.5	19.3
		Middle	158.1	151.0	165.8	114.8
(122)		Upper	406.8	360.0	417.5	294.3
	S2MSI	-	12.2	9.6	15.3	7.1
136.8	NHN	-	21.5	20.9	27.2	11.2
Riviere Rouge	2014NRC database	Lower	66.2	60.4	79.1	-67.3
		Middle	35.3	43.0	45.8	13.0
(64)		Upper	128.3	193.8	135.6	131.3
	S2MSI	-	15.6	19.4	18.3	-11.9
97.7	NHN	-	11.3	14.1	14.0	-8.1
Ottawa River	2014NRC database	Lower	1200.5	87.2	1298.5	-88.9
		Middle	1040.5	73.6	1152.2	-77.1
(45)		Upper	700.5	44.7	857.7	-51.9
	S2MSI	-	29.7	2.7	39.8	0.3
1350.5	NHN	-	268.0	40.9	512.1	28.0

4.2 Hydrokinetic Energy Estimates

The updated HK power dataset provides estimates of HK power, including AEP and power for each flow exceedance, for every location except for the Arctic region because of a lack of discharge data in the Arctic, as illustrated in Figure 15. It is important to note that the new database is less continuous compared to the previous 2014NRC dataset because it does not provide power estimates for lakes and reservoirs. This is because the velocity of water in lakes and reservoirs is typically not high enough for efficient HK energy extraction. As a result, the focus was solely on deriving power estimates for rivers in the updated dataset.

Despite the reduced continuity, the updated database brings significant improvements in resolution and accuracy for HK power estimates. Figure 16 illustrates the improved resolution and the ability of the dataset to identify specific areas of high HK energy potential. Notably, the dataset can now identify locations of high HK power attributed to width constrictions in rivers. However, it is important to highlight that the updated database does not account for local increases in velocity and HK power caused by other factors, such as changes in depth or slope, beyond what was already provided by the resolution and accuracy of the 2014NRC database.

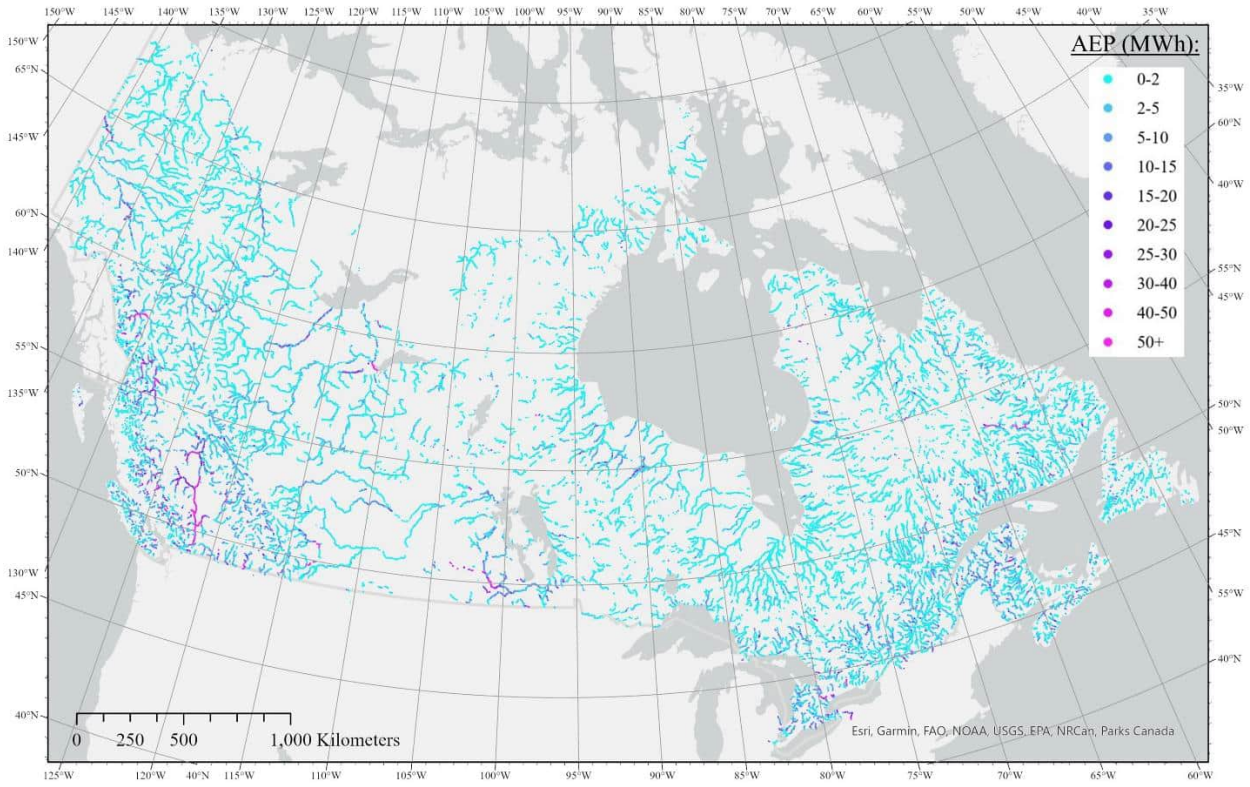

Figure 15: Hydrokinetic power estimates across Canada.

Figure 16: Hydrokinetic power estimates illustrating the resolution of the updated dataset.

The general trend of HK power distribution in the country is that most promising resources are located in British Columbia (Figure 15). In particular, the Fraser River falls within the 50+ MWh range for most of its length. Additionally, the Thompson River, Thompson River, Stikine River, Nass River, Skeena River, and West Road (Blackwater) River (locations illustrated in Figure 31) show promising HK power resources for much of their length. Rivers in the St. Lawrence, Northern Quebec, and Labrador watersheds are also promising for HK power; however, the promising locations are less continuous, and cases like that of Figure 16 are more common.

On the other hand, areas with low slope, such as the prairies, central Northwest Territories, and east Yukon, are less likely to have promising HK power resources in rivers, as the large rivers in these locations tend to become braided.

Upon observation, many high HK power locations corresponding with a width constriction are associated with some type of white-water conditions. However, some locations with width constrictions did not lead to white water conditions. In these locations, the flow may be restricted laterally by bedrock or similar material but not constricted vertically, so deepening of the channel may be present. Until methods and data improve enough to produce estimates of river depth, such differences in riverbed depth and their effect on HK power will not be able to be captured in the dataset. Additionally, some observed areas of white water did not have high HK power estimates in the database, and this is because the white water and associated high velocity conditions were caused by a high slope or by a depth constriction.

5 Discussion

The newly developed width datasets – from both the NHN and from S2MSI imagery – were shown to be more accurate than the previous estimates of river width from the 2014NRC database, especially in large rivers that the 2014NRC database tended to under-estimate. NHN-derived widths contained less error than the imagery-derived widths located at smaller rivers, mostly due to the limitations of the imagery resolution. Conversely, the imagery-based method was able to improve the accuracy of width measurements compared to the NHN-derived widths in larger rivers, because the NHN-derived width is representative of only a single flow condition and may not represent the range of expected river widths. For example, the Ottawa River validation area in Table 3 included a shallow sand bar and shallow vegetated area. The NHN polygons depicted this area to be inundated, but the coinciding S2MSI and high-resolution polygons represented a flow condition in which these areas were not inundated. Thus, a future comparison of NHN-derived widths and imagery-derived widths across all of Canada will be a valuable exercise to identify locations where NHN water polygons may not be representative of the range of expected channel widths. Within major WS1, the MAPE between the imagery-derived widths and NHN-derived widths was 18.2% and the mean percent error (MPE) was -13.3%, indicating that the imagery-based method, on average, estimates river widths to be smaller than the NHN-based method of width estimation.

The relationship between imagery-derived width and flow exceedance was found to be weak in major WS1, so average imagery-derived width was used, and lower and upper limits of power were calculated by using the maximum of the imagery-derived widths and minimum imagery-derived widths, respectively. The weakness of the relationship was likely, in part, caused by the stationary threshold and uniform method of extracting surface water from satellite imagery. A trend was observed in the surface water extracted from satellite imagery where the month of October sometimes contained disjointed waterbodies. When the threshold was decreased (i.e., from -0.3 to -0.4 or -0.5), these known watery pixels were then successfully identified as surface water. Preliminary analyses indicated that these discrepancies may have been caused by seasonal changing of the solar radiation intensity; however, additional analysis is required to fully define sources of the error/discrepancy. Additionally, this methodology assumes that the widths extracted from four satellite images selected within a month can be averaged and that value will represent the month-averaged river width. However, these images may not have necessarily been captured during the “monthly average condition”. For example, if a rainstorm occurred in July or August, and an image was used that captured the width during that event, it would skew the month-averaged width to be higher than the actual average. Alternatively, if freshet occurred earlier than average in a particular year, the month-representative calculated width for June may be smaller than the actual value. This skew would be more likely for areas where only one or two images could be used, due to cloud cover and snow/ice.

Upon comparing the previous 2014NRC database (shown in Figure 17) to the updated database, the two databases satisfy two different purposes. The updated database, with its improved resolution, can identify specific locations of high HK power potential due to width constrictions. As such, developers and communities can use the updated dataset to find specific locations of high HK energy potential, rather than identifying promising reaches as was done in the 2014NRC dataset. The 2014NRC database provides more continuity of flow and includes small rivers, creeks, and irrigation systems, whereas the updated database does not include these small waterbodies. As such, the 2014NRC database provides a better representation of the total HK power in Canada.

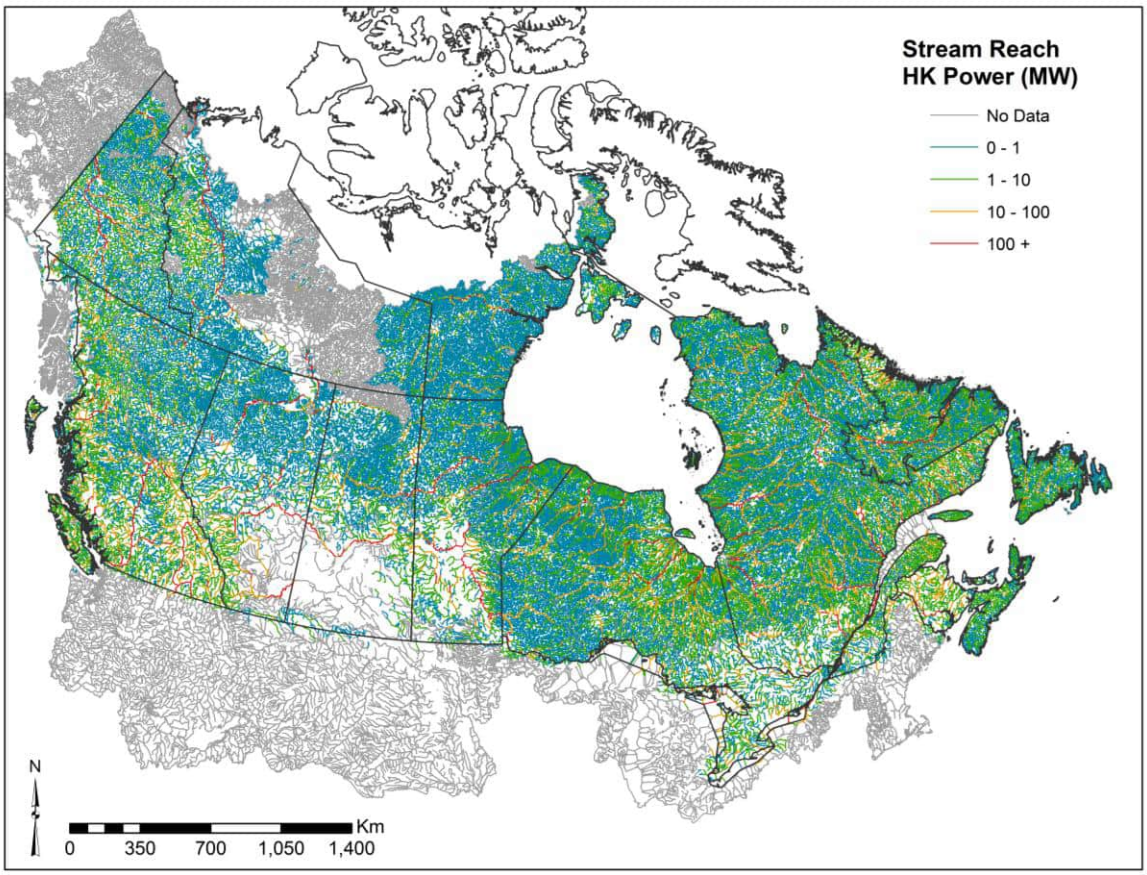

Figure 17: Hydrokinetic power estimates across Canada from the previous 2014NRC database.

The updated data, when compared to validation data from a case study on the Riviere Rouge [41] that used field data collection and hydrodynamic modelling to estimate the AEP, has demonstrated higher accuracy than the previous 2014NRC dataset. The validation exercise used HK power estimates calculated from field measurements and a calibrated hydrodynamic model. The comparison of the validation data with estimates from the updated database showed that the new dataset provides more accurate estimates of HK power. The validation data were compared to estimates from the updated database; the closest database point is located 350m upstream of the case study location (see Figure 18). The results of the comparison are presented in Table 4. HK power estimates at this location were based on widths derived from the NHN database. The 2014NRC database slightly underestimated the mean AEP, and the high range of the AEP in the NRC2014 dataset was underestimated. The new database overestimated the AEP; however, this may be caused by the 350m separation between the database point and the case study location. The validation data is located at an area where the river width is approximately 65m, and the updated database point is located at an area with a river width of 45m. If the new value of a width of 65m is used in the AEP calculation, 10.8 MWh is expected, which is closer to the validation data value. As shown in Table 3, the width estimate of this location in the previous 2014NRC dataset is quite close to the measured value, which contributes to a successful AEP calculation at this location. However, for other locations where the width estimate in the 2014NRC dataset is not accurate (see Table 3), one can suspect that the newly developed dataset will produce a more accurate AEP than the 2014NRC dataset.

Figure 18: Location of validation data compared to updated database point.

Table 4: Comparison and validation of previous 2014NRC database and newly developed database at Riviere Rouge, QC, location

FE [%]	2014NRC [W]	New database [W]	Validation data
0.01	10859	71038	-
0.1	7542	48962	-
0.5	4692	40059	-
1	4158	29251	-
5	2258	14412	-
10	1518	8072	-
20	679	3179	-
30	446	2223	-
40	261	1492	-
50	194	972	-
60	126	755	-
70	82	474	-
80	71	355	-
90	49	297	-
95	39	174	-
99	0	0	-
99.9	0	0	-
AEP [MWh]			
Mean	4.8	28.3	6.2
High	9.8	-	21.8
Low	2.4	-	-

Currently, the database relies on measurements of river width from the NHN polygons in all watersheds but major WS1. It was observed that the NHN polygons sometimes poorly represent river waterbodies in the Prairies (particularly Alberta) and the Yukon for the following reasons. The NHN polygons are sometimes not representative of the current river location (if the river has meandered or changed shape), and some NHN polygons are too narrow compared to the actual river and underestimate the river width, thus overestimating the HK power. Additionally, the current methods of estimating velocity assume that the river flow is confined within the measured width for all flow exceedances. This is unlikely specifically for flows above the bankfull flow condition, which is expected to be exceeded above the 1.5-year return period (approximately 0.2% flow

exceedance). The 0.1% and 0.01% exceedance flows will likely overtop the banks of the river and spill into the floodplain. This is especially true for rivers not confined within canyons or bedrock. Thus, a review of the relationship between flood conditions, river velocity, and river width should be conducted for compound channels to understand how velocity should be estimated using the available data in flooded conditions.

It was also observed that flow estimates from the 2014NRC database are sometimes greatly overexaggerated in meandering rivers in the Prairies and in central Northwest Territories, leading to great overestimation of HK power in these rivers, as observed in the updated HK database. A summary is provided in Table 5 of various locations of overestimated flow in the 2014NRC database compared to gauged flow data. The locations of the gauges and the datapoints in the new database are illustrated in Figure 19. There does not seem to be a trend when comparing the criteria of the gauged data at each location (i.e., whether the data is continuous or seasonal, whether the data is discontinued or active, etc.) to understand if the gauge station characteristics contributed to whether or not the flow was overestimated in the 2014NRC dataset. Table 5 illustrates that the flows in these rivers were overestimated in the NRC2014 dataset regardless of the seasonality or activeness of the adjacent gauges. As such, it is not clear if the quality of the gauged flow data contributed to the overestimation of flows in the NRC2014 database. These rivers with overestimated flows are all located in underfit rivers (i.e., rivers too small for the valley in which they flow [42]), so the previous methods used to develop the flow estimates for the 2014NRC database may have overestimated small rivers located in large glacial valleys.

Table 5: Comparison between 2014NRC database and flow statistics derived from WSC gauges at locations with high HK power estimation error

River	**Assiniboine River**	**Assiniboine River**	**Assiniboine River**	**Qu'Appelle River**
Location	Near Russell, MB, Active, Continuous	Near Miniota, MB, Active, Seasonal	Near Brandon, MB, Active, Continuous	Below Katepwa Lake, SK, Discontinued
Latitude, Longitude	50.810056, -101.435361	50.110611, -101.037944	49.861444, -99.961583	50.661389, -103.600556
Station #	05ME001	05ME006	05MH001	05JL001
Years	1913-2020	1954-2020	1906-2020	1911-1998
0.01% Flow Exceedance, 2014NRC	887	2886	3731	15556
0.01% Flow Exceedance, Gauge	493	944	1010	80
50% Flow Exceedance, 2014NRC	1.1	0.4	0.5	0
50% Flow Exceedance, Gauge	6.7	17.0	12.6	2.9

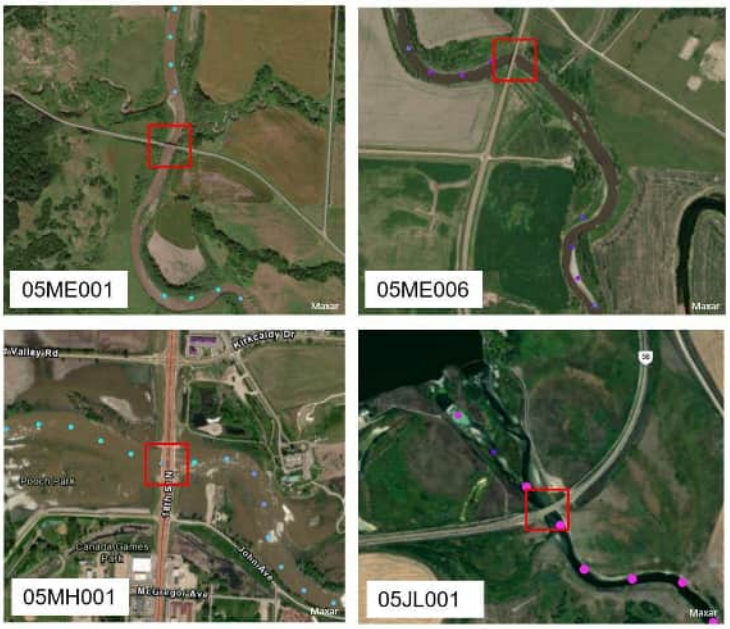

Figure 19: Location of WSC gauges used for error analysis.

5.1 Limitations

Estimating HK power resources in the Arctic with flow estimates from Tuefel and Sushama [20] and depth estimates from the 2014NRC database was not yet completed for this report. Such estimates will be available upon the release of the next version of the updated HK database and the subsequent version of this report.

The widths derived from the NHN water polygons only represent one flow condition, and it is not possible to determine this flow condition as the NHN metadata do not link the water polygons to a specific date or timeframe. As such, the NHN-derived widths provide a good first estimate of width that is more accurate than the widths from the NRC2014 dataset and can be improved further. Additionally, the NHN polygons were observed to poorly represent the actual river shape and width in some locations (see Figure 24). HK power can be exaggerated or understated based on the widths extracted from the NHN polygons. In Figure 20, the two datapoints in the lower left corner of the image have an overestimated AEP (thus the darker colour of the points) due to the smaller river width represented by the NHN polygon. In general, the NHN polygons poorly represented river waterbodies in central NWT (NHN watershed 7), southern Yukon (NHN watershed 9), and the Prairies (NHN watershed 5). As such, it is expected that imagery-derived widths will improve the width estimates in these locations. However, in locations where an imagery-derived width cannot be extracted from S2MSI imagery, due to resolution restrictions, the HK power may be overestimated if the NHN-derived widths are smaller than the actual river width.

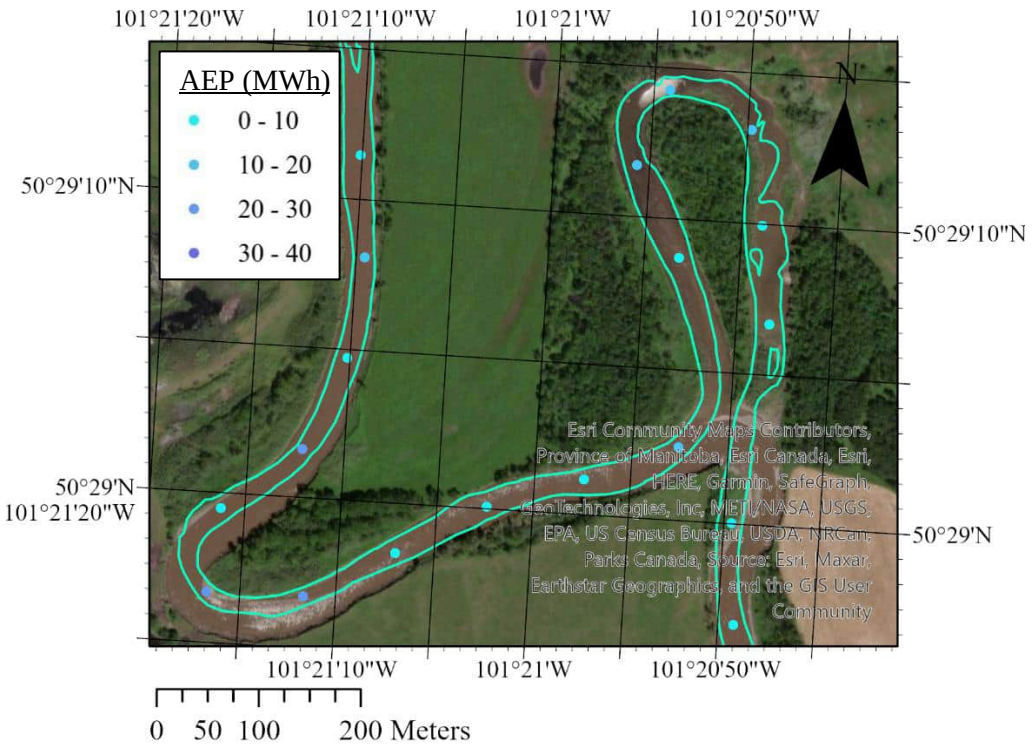

Figure 20: Example where NHN polygons poorly represent the actual Assiniboine River waterbody and channel width leading to erroneous HK power estimation

When extracting widths from S2MSI imagery, filters were applied to exclude images over a certain cloud and snow/ice percentage. Additionally, cloud masks were applied to imagery that fell within the total cloud cover percentage criteria to remove specific cloud and cloud shadow areas. Consequently, although each point may have up to a maximum of 24 width measurements, many points have fewer measurements than 24, and some don't have any measurements. This limits the applicability of the imagery-based width estimation. Width measurements will become fewer in areas with snow/ice later in spring and earlier in fall as well as areas that are often cloud covered (e.g., Pacific coast). With the combination of NHN-based and imagery-based widths in the database, each point should at least have one width measurement available.

Imagery-derived widths could not be applied as expected (i.e., by capturing changes in river width and producing WDCs). However, it is expected that this method of directly measuring the river width from either the NHN polygons or from S2MSI imagery provides a more accurate representation of channel width (as presented in Table 3 and Figure 13) and a more detailed representation of width variation along the channel compared to the 2014NRC database, despite the inability to capture width variability for multiple flow conditions. Future work will include further analysis of the effects of seasonal surface reflectance and cloud cover on the accuracy of the S2MSI imagery classification methods. This analysis will be completed on the remaining ten watersheds, as the imagery-derived width analysis was completed only on major WS1 for this iteration of the national hydrokinetic energy database. If the relationship between imagery-derived river width and flow exceedance can be strengthened in future work based on the aforementioned analysis, WDCs could be developed and applied with confidence. In the calculation of HK power in this report, the mean of the imagery-derived width was one of the values used to convert flow to velocity. In using the mean width to calculate velocity, the highest velocities would be over-estimated, and the lowest velocities would be underestimated, as river width generally increases with increasing flow and velocity. This simplification is likely to cause an over-estimation of final HK power, as velocity is cubed in the kinetic power equation so the higher exceedance points on the PDC will be overstated.

The regionalization method used by Jenkinson and Bomhof [14] to estimate river depth was not able to capture depth constrictions, such as bedrock sills that could create favorable conditions for river HK energy generation. With the availability of altimetry data improving world-wide, improved depth estimates may be possible in the future when altimetry data is accessible at a national-scale [10], [16].

5.2 Future Work

The HK energy resource database will be updated further beyond the results presented in this report. The Arctic is an area of high interest in terms of HK energy resource estimation. Flow estimates will be applied to the database points in the Arctic from the Tuefel and Sushama [20] dataset. Because of the observed errors from the 2014NRC flow data, the flow estimates derived by Tuefel and Sushama [20] will also be applied everywhere in Canada, as they likely do not overestimate flow in overfit streams to the extent that the previous 2014NRC dataset does. Additionally, depth estimates will be derived in the Arctic using the same regionalization techniques applied by Jenkinson and Bomhof [14]. With these updates, river velocity can be estimated, and the resulting AEP will be calculated.

Although the imagery-derived widths show promising results to improve the accuracy beyond the 2014NRC database as well as the NHN-derived widths, further analysis needs to be performed in major WS1 to optimize the extraction of river widths from S2MSI imagery. Analysis of the effects of adjusting the threshold seasonally, based on solar radiation and surface reflectance, is expected to improve imagery-derived width accuracy. Overall, this is expected to strengthen the relationship between imagery-derived width and flow exceedance percent; thus, it may be possible to develop imagery-derived WDCs in the future analysis.

Imagery-derived widths will be generated for Canada in the other ten watersheds, as only major WS1 including New Brunswick, Nova Scotia, Prince Edward Island, and part of Quebec was analyzed in this work. After optimization of the processing of S2MSI imagery in major WS1, GEE will be used to perform cloud-based satellite imagery pre-processing, mosaicking, spectral index-based classification, and export for all other major watersheds. Imagery-derived widths will be applied to the final AEP where they exist, although the information related to AEP calculation using the NHN-derived width will be available for all datapoints. Additionally, because it is unlikely that the flow above bankfull flow will be contained within the channel width calculated from either imagery or the NHN, a review of the relationship between flood conditions, river velocity, and river width will be conducted for compound channels to understand how velocity should be estimated using the available data in flooded conditions.

When the final HK power resource estimates are available after optimizing the imagery-derived width generation procedure, generating imagery-derived widths in all watersheds, and calculating power estimates in the Arctic, the spatial distribution of HK power resource will be evaluated. Updated power estimates will also be compared to the previous 2104NRC estimates. Finally, the power estimates from this analysis will be validated further through comparison with power estimates derived from field measurements and hydrodynamic modelling [41].

6 Conclusions

Both the NHN-derived and the imagery-derived widths were able to substantially improve measurements of river width from the previous 2014NRC database. NHN-derived widths were observed to be accurate for small rivers, and imagery-derived widths were likely to be more accurate for larger rivers. Imagery-derived width generation needs to be optimized in future work to better understand the feasibility of linking imagery-derived widths to flow exceedance conditions to develop WDCs. Otherwise, a mean imagery-derived width can be used, but the maximum and minimum imagery derived widths should also be used in the calculation of HK power to provide a lower and upper limit of power, respectively. In the future updated HK power database, at least one updated width value will be available for each point in the database, either from the NHN or from S2MSI imagery. This will be based on the availability of S2MSI imagery in certain locations which is contingent on the imagery meeting cloud cover and snow/ice criteria.

The newly developed database and the previous 2014NRC database serve different purposes. The continuity of the 2014NRC database allows for calculation of the total HK power in the country and by region. The newly developed database allows users to better identify localized areas of potentially high HK power availability associated with width constrictions along the channel. The database illustrates that the most promising HK power locations are in British Columbia where the flow is constrained in canyons or by high slope landforms. However, less continuous datapoints with high HK power estimates are found throughout the St. Lawrence, Northern Quebec, Labrador, and Albany watersheds. The imagery-derived widths are expected to improve HK power estimates in future work, as the NHN polygons poorly represented the shape of river waterbodies in some locations across the country.

To update the national HK database beyond what has been developed already, the river flow estimates that are available for the Arctic should be applied to the existing database points generated for the rivers in the Arctic. Additionally, in the Arctic, depth estimates should be calculated by utilizing the regression techniques used in the previous 2014NRC HK energy database. With both of these attributes and the river width data estimated thus far, it should be possible to estimate HK power for Arctic regions. To improve the accuracy of imagery-derived width estimates, the method of extracting surface water from S2MSI imagery should be optimized by analyzing the effects of limiting the cloud cover filtering and masking as well as attempting seasonal-based thresholding. Finally, validation of the final power estimates in the database should be conducted using power calculated in specific locations that have been hydrodynamically modelled using field collected data.

7 Acknowledgements

The authors are grateful for and would like to acknowledge the expertise provided by Richard Burcher in the satellite image processing and GIS aspects of the project. The authors would also like to acknowledge the expertise and advice provided by James Bomhof in the hydraulic geometry aspects of the project as well as in utilizing the 2014NRC database in this work.

The authors would also like to acknowledge the funding provided by the Highly Qualified Personnel (HQP) Grant from the National Research Council of Canada (NRC) Collaborative Science, Technology and Innovation Program (CSTIP).

8 References

[1] Intergovernmental Panel on Climate Change, “Synthesis report of the IPCC sixth assessment report (AR6),” 2023.

[2] Environment and Climate Change Canada, *2030 Emissions Reduction Plan – canad’s Next Steps for Clean Air and a Strong Economy*. Gatineau, QC, 2022.

[3] United Nations, “Paris Agreemnt,” 2015.

[4] Natural Resources Canada, *Energy Fact Book 2022-2023*. 2022. [Online]. Available: https://natural-resources.canada.ca/sites/nrcan/files/energy/energy_fact/2022-2023/PDF/Energy-factbook-2022-2023_EN.pdf

[5] I. G. Baird *et al.*, “The Downstream Impacts of Hydropower Dams and Indigenous and Local Knowledge: Examples from the Peace–Athabasca, Mekong, and Amazon,” *Environ. Manage.*, vol. 67, pp. 682–696, 2021, doi: 10.1007/s00267-020-01418-x.

[6] C. R. Schilt, “Developing fish passage and protection at hydropower dams,” *Appl. Anim. Behav. Sci.*, vol. 104, no. 3–4, pp. 295–325, 2007, doi: 10.1016/j.applanim.2006.09.004.

[7] J. Singer and T. Watanabe, “Reducing reservoir impacts and improving outcomes for dam-forced resettlement: experiences in central Vietnam,” *Lakes Reserv. Res. Manag.*, vol. 19, no. 3, pp. 225–235, 2014, doi: 10.1111/lre.12072.

[8] A. Soukhaphon, I. G. Baird, and Z. S. Hogan, “The Impacts of Hydropower Dams in the Mekong River Basin: A Review,” *Water*, vol. 13, no. 3, p. 265, 2021, doi: 10.3390/w13030265.

[9] H. F. Yang *et al.*, “Human impacts on sediment in the Yangtze River: A review and new perspectives,” *Glob. Planet. Change*, vol. 162, pp. 8–17, 2018, doi: 10.1016/j.gloplacha.2018.01.001.

[10] K. Kirby, S. Ferguson, C. D. Rennie, I. Nistor, and J. Cousineau, “Investigation of Methods to Improve Canada’s Hydrokinetic Energy Resource Database, Literature Review.” National Research Council Canada - Ocean, Coastal and River Engineering, 2020.

[11] K. Kirby, C. Rennie, J. Cousineau, S. Ferguson, and I. Nistor, “Riverine hydrokinetic energy extraction: Investigation into a location’s suitability for turbine deployment,” in *Proceedings of the Canadian Society of Civil Engineering Annual Conference 2021*, 2021. doi: https://doi.org/10.1007/978-981-19-1065-4_56.

[12] K. Kirby, C. Rennie, I. Nistor, J. Cousineau, and S. Ferguson, “Investigation into the Influence of Flow Variation on Estimated Available Riverine Hydrokinetic Energy by Modelling a Reach of the Rouge River, Quebec, Canada,” in *Proceedings of the 39th IAHR World Congress*, International Association for Hydro-Environment Engineering and Research (IAHR), 2022. doi: 10.3850/IAHR-39WC2521711920221251.

[13] IEC, “Marine energy - Wave, tidal and other water current converters - Part 301: River energy resource assessment,” International Electrotechnical Commission, Geneva, Switzerland, Technical Specification 62600–301, Edition 1.0, 2019.

[14] W. Jenkinson and J. Bomhof, “Assessment of Canada’s Hydrokinetic Power Potential. Phase III Report: Resource Estimation.” National Research Council Canada, Ottawa, ON, Canada, 2014.

[15] M. N. Khaliq and J. Cousineau, “Assessment of Canada’s Hydrokinetic Resources: A Review of Hydrologic Considerations,” National Research Council Canada, NRC-OCRE-2020-TR-019, 2020.

[16] K. Kirby, S. Ferguson, C. Rennie, I. Nistor, and J. Cousineau, “Assessments of Available Riverine Hydrokinetic Energy: A Review,” *Can. J. Civ. Eng.*, 2021, doi: https://doi.org/10.1139/cjce-2021-0178.

[17] Natural Resources Canada, “Atlas of Canada 1,000,000 National Frameworks Data, Hydrology - Drainage Network Version 6.0.” 2008. [Online]. Available: https://ftp.maps.canada.ca/pub/nrcan_rncan/archive/vector/framework_cadre/hydrology/analytical/drainage_network/

[18] J. Bomhof, “Estimating Flow, Hydraulic Geometry, and Hydrokinetic Power at Ungauged Locations in Canada,” Master of Applied Science in Engineering Thesis, University of Ottawa, The Ottawa-Carleton Institute for Civil Engineering, Department of Civil Engineering, 2014.

[19] R. W. Jenkinson and J. Bomhof, “Assessment of Canada’s Hydrokinetic Power Potential: Phase II Report Methodology Validation,” National Research Council Canada, Ottawa ON, 2012.

[20] B. Teufel and L. Sushama, “Hydrokinetic resource estimation for the Canadian Arctic – Phase I,” Department of Civil Engineering and Trottier Institute for Sustainability in Engineering and Design, McGill University, Technical Report, 2022.

[21] L. Sushama, B. Teufel, J. Atrill, A. Faki, V. Poitras, and L. Duarte, “Engineering climate simulations and thresholds for Nunavut,” Climate Change Adaptation and Planning Group of Transport Canada, Technical Report, 2021.

[22] L. B. Leopold and T. Maddock, “The Hydraulic Geometry of Stream Channels and Some Physiographic Implications,” United States Department of the Interior, Washington D.C., Geological Survey Professional Paper 252, 1953.

[23] D. Knighton, *Fluvial Forms and Processes*. London, U.K.: Edward Arnold Ltd., 1984.
[24] M. G. Wolman and J. P. Miller, “Magnitude and Frequency of Forces in Geomorphic Processes,” *J. Geol.*, vol. 68, no. 1, pp. 54–74, 1960, doi: 10.1086/626637.
[25] R. Copeland, D. Biedenharn, and J. Fischenich, “Channel-forming discharge,” US Army Corps of Engineers, 2000.
[26] Natural Resources Canada; Government of Canada, “National Hydro Network - NHN - GeoBase Series - Open Government Portal,” 2017. https://open.canada.ca/data/en/dataset/a4b190fe-e090-4e6d-881e-b87956c07977 (accessed Sep. 20, 2022).
[27] ESA, TAS Team, “Sentinel-2 Products Specification Document,” S2-PDGS-TAS-DI-PSD, 2021. [Online]. Available: https://sentinel.esa.int/documents/247904/4756619/S2-PDGS-TAS-DI-PSD-V14.9.pdf/3d3b6c9c-4334-dcc4-3aa7-f7c0deffbaf7
[28] ESA, “Sentinel-2 MSI: Level-2A,” n.d. https://sentinels.copernicus.eu/web/sentinel/user-guides/sentinel-2-msi/product-types/level-2a (accessed May 18, 2023).
[29] ESA, “User Guides - Sentinel-1 SAR - Sentinel Online.” https://sentinel.esa.int/web/sentinel/user-guides/sentinel-1-sar (accessed Nov. 30, 2022).
[30] K. Kirby, S. Ferguson, C. D. Rennie, J. Cousineau, and I. Nistor, “(Draft) Comparison of satellite image surface water detection methods in four diverse locations using two criteria: total waterbody area and widths of rivers,” *Be Submitt. Remote Sens.*, 2023.
[31] G. L. Feyisa, H. Meilby, R. Fensholt, and S. R. Proud, “Automated Water Extraction Index: A new technique for surface water mapping using Landsat imagery,” *Remote Sens. Environ.*, vol. 140, pp. 23–35, Jan. 2014, doi: 10.1016/j.rse.2013.08.029.
[32] ESA, “Sentinel-2 Mission Guide,” n.d. https://sentinel.esa.int/web/sentinel/missions/sentinel-2 (accessed May 18, 2023).
[33] ESA, “Sentinel-2 MSI: MultiSpectral Instrument (MSI) Overview,” n.d. https://sentinels.copernicus.eu/web/sentinel/technical-guides/sentinel-2-msi/msi-instrument (accessed May 18, 2023).
[34] J. Chen *et al.*, “Global land cover mapping at 30m resolution: A POK-based operational approach,” *ISPRS J. Photogramm. Remote Sens.*, vol. 103, pp. 7–27, 2015, doi: 10.1016/j.isprsjprs.2014.09.002.
[35] C. Huang *et al.*, “Land Cover Mapping in Cloud-Prone Tropical Areas Using Sentinel-2 Data: Integrating Spectral Features with Ndvi Temporal Dynamics,” *Remote Sens. Basel Switz.*, vol. 12, no. 7, pp. 1163-, 2020, doi: 10.3390/rs12071163.
[36] T. M. Pavelsky and L. C. Smith, “RivWidth: A Software Tool for the Calculation of River Widths From Remotely Sensed Imagery,” *IEEE Geosci. Remote Sens. Lett.*, vol. 5, no. 1, pp. 70–73, Jan. 2008, doi: 10.1109/LGRS.2007.908305.
[37] B. Nyberg, S. Buckley, J. Howell, and R. Nanson, “Geometric Attribute and Shape Characterization of Modern Depositional Elements: A Quantitative GIS Method for Empirical Analysis,” *Comput. Geosci.*, vol. 82, Jun. 2015, doi: 10.1016/j.cageo.2015.06.003.
[38] Sentinel-Hub, “Sentinel-2 L2A,” *About Sentinel-2 L2A Data*, Mar. 29, 2023. https://docs.sentinel-hub.com/api/latest/data/sentinel-2-l2a/ (accessed Mar. 28, 2023).
[39] ESRI, “ArcGIS Pro: Spatial Join (Analysis).” https://pro.arcgis.com/en/pro-app/latest/tool-reference/analysis/spatial-join.htm (accessed Mar. 31, 2023).
[40] L. B. Leopold, *A view of the river*. Cambridge, Mass: Harvard University Press, 1994.
[41] K. Kirby, “Impacts of seasonal flow variation on riverine hydrokinetic energy resources and optimal turbine location – Case study on the Rivière Rouge, Québec, Canada,” *Renew. Energy*, Apr. 2023, doi: 10.1016/j.renene.2023.04.067.
[42] G. H. Dury, “Principles of Underfit Streams,” USGS, Geological Survey Professional Paper 452-A, 1964.

Appendix A

A.1 Google Earth Engine script to process and extract Sentinel-2 imagery (Javascript)

```
/**
 * Function to mask clouds, cloud shadow, snow/ice using the Sentinel-2 SCL
band
 * @param {ee.Image} image Sentinel-2 image
 * @return {ee.Image} cloud masked Sentinel-2 image
 */

function s2ClearSky(image) {
      var scl = image.select('SCL');
      var clear_sky_pixels =
scl.eq(2).or(scl.eq(4)).or(scl.eq(5)).or(scl.eq(6)).or(scl.eq(7));
      return image.updateMask(clear_sky_pixels).divide(10000);
};

//call Sentinel-2 catalogue and set filtering parameters
var dataset = ee.ImageCollection('COPERNICUS/S2_SR_HARMONIZED')
                  .filterDate('2022-10-01', '2022-10-31')
                  // Pre-filter to get less cloudy granules.
                  .filter(ee.Filter.lt('CLOUDY_PIXEL_PERCENTAGE',20))
                  .filter(ee.Filter.lt('SNOW_ICE_PERCENTAGE',0.1))
                  .map(s2ClearSky);

//set map parameters to visualize the false colour image
var visualization = {
  min: 0.0,
  max: 0.3,
  bands: ['B4', 'B3', 'B2'],
};

Map.setCenter(83.277, 17.7009, 12);

Map.addLayer(dataset.mean(), visualization, 'RGB');

//mosaic Sentinel-2 imagery to process and extract
var mosaic = dataset.mosaic();

//resampling
var proj = mosaic.projection().getInfo();
var crs = proj['crs'];
var mosaic_10m = mosaic.reproject({'crs': mosaic.select([0]).projection(),
'scale': 20});

//calculating AWEI_NSH
var AWEI = mosaic_10m.expression(
      '(4 * (GREEN - SWIR1) - 0.25 * NIR - 2.75 * SWIR2)', {
      'NIR': mosaic_10m.select('B8'),
      'SWIR1': mosaic_10m.select('B11'),
      'SWIR2': mosaic_10m.select('B12'),
      'GREEN': mosaic_10m.select('B3')
});
```

```
//calculating NDWI to compare to AWEI
var NDWI = mosaic_10m.expression(
      '((GREEN - NIR)/(GREEN + NIR))', {
      'NIR': mosaic_10m.select('B8'),
      'GREEN': mosaic_10m.select('B3')
});


//set map visualization parameters
Map.setCenter(-66.80579617700961, 45.9675524874753, 11);

Map.addLayer(AWEI, {min: -1, max: 1, palette: ['a6611a', 'f5f5f5',
'4dac26']}, 'AWEI');
Map.addLayer(NDWI, {min: -1, max: 1, palette: ['a6611a', 'f5f5f5',
'4dac26']}, 'NDWI');

//thresholding of AWEI and NDWI
var water_AWEI = AWEI.gt(-0.3);
var water_NDWI = NDWI.gt(-0.1);

//visualize thresholded AWEI result
Map.addLayer(water_AWEI, {min: -1, max: 1, palette: ['a6611a', 'f5f5f5',
'4dac26']}, 'water_AWEI');

//visualize threshold NDWI result to compare to AWEI
Map.addLayer(water_NDWI, {min: -1, max: 1, palette: ['a6611a', 'f5f5f5',
'4dac26']}, 'water_NDWI');

//export thresholded AWEI result to Google Drive
//remember to adjust max pixels based on location
Export.image.toDrive({
  image: water_AWEI,
  description: '10_2022_awei_watershed01_2',
  folder: 'ee_AWEI_exports',
  region: geometry,
  scale: 20,
  maxPixels: 2000000000
});
```

A.2 Analysis of the relationship between imagery-derived widths and flow exceedances

A.2.1 Methods

To link imagery-derived river widths to flow exceedances in an attempt to develop width duration curves (WDC), the trend of the month-average flow exceedance was compared to the imagery-derived widths. The database points with width information and the gauge station points with flow exceedance information were spatially joined using the NHN drainage basin polygons. The NHN drainage area polygons are divided into three resolutions: the lowest resolution drainage basins are the major watersheds of which there are eleven (corresponding to the first number in the gauge station label, **01**AA000), the medium resolution drainage basin is the sub-drainage basin illustrated on the left in Figure 21 (corresponding to the first letter in the gauge station label, 01**A**A000), and the highest resolution drainage basin is the subsub-drainage basin (corresponding to the

second letter in the gauge station label, 01A**A**000) illustrated on the right in Figure 21. The last three numbers in the gauge station label correspond to the individual gauge station (01AA**000**).

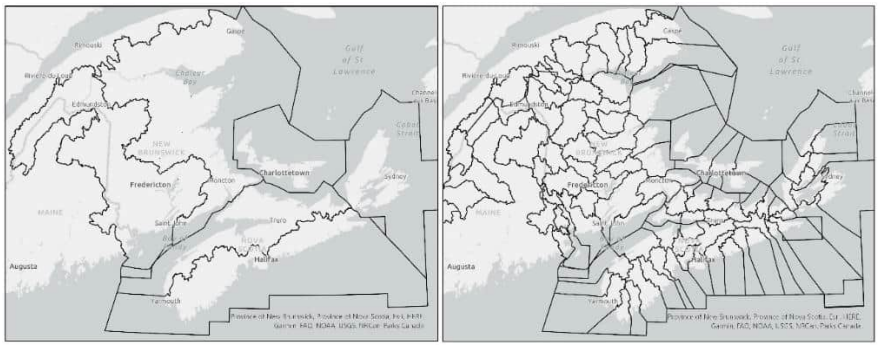

Figure 21: (Left) Sub-drainage basins and (right) subsub-drainage basins for major WS1 in the NHN and WSC databases.

For WSC gauges with continuous and recent (last 20 years) data, FDCs were developed, and daily flows were averaged for the months of May, June, July, August, September, and October. The flow exceedance corresponding to the month-averaged flows was then calculated. The resulting values were month-averaged flow exceedances corresponding to the month-averaged imagery-derived widths. Figure 22 illustrates the gauge stations that met the criteria outlined above, the blue subsub-drainage basins contain at least one viable gauge station, and pink areas did not contain a viable gauge station. In each blue area, the mean of the month-averaged flow exceedances was calculated. For example, if one area contained three viable gauge stations, the three month-averaged May exceedances would be averaged, the three month-averaged June exceedances would be averaged, etc. In the pink areas, the resolution of the grouping was increased to sub-drainage basin and the month-averaged flow exceedances were spatially averaged using the polygons on the left side of Figure 21.

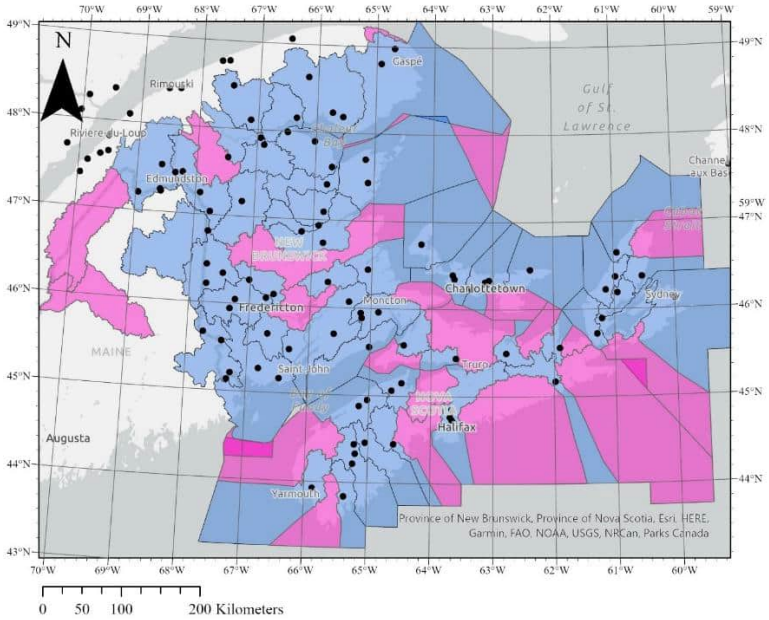

Figure 22: Subsub-drainage basins in the NHN and WSC discharge database with gauge stations that met the minimum criteria in blue and areas that did not in pink. Gauge station locations that met the criteria shown as black circles.

An analysis was performed on the impact of spatially grouping the flow exceedance information by different resolution polygons (entire watershed vs. sub-drainage basins vs. subsub-drainage basins). The effect of this

spatial grouping and averaging was represented by the variance and standard deviation of the data. As shown in Table 6, grouping the data by highest possible resolution was expected to reduce the variance and standard deviation; thus, grouping by highest resolution would be expected to reduce the error. As such, previously described tiered approach was applied where database width points that fell within a subsub-drainage basin with at least one viable gauge station would be linked to the mean of the month-averaged flow exceedances of that subsub-drainage basin. Database width points that did not fall within a viable subsub-drainage basin would instead be linked to the mean of the month-averaged flow exceedances of the sub-drainage basin that they fell within.

Table 6: Variances (VAR) and standard deviations (STDEV) of flow exceedances at different resolutions of grouping gauge stations.

Resolution	Method	May	June	July	August	September	October
All gauges	VAR	1.99%	2.88%	4.28%	4.23%	3.06%	1.52%
	STDEV	14.10%	16.97%	20.68%	20.57%	17.49%	12.31%
Entire WS1	VAR	1.10%	1.21%	1.64%	1.27%	1.26%	1.01%
	STDEV	10.51%	10.99%	12.83%	11.28%	11.23%	10.04%
Sub-drainage basins	VAR	0.32%	0.36%	0.37%	0.58%	1.02%	0.92%
	STDEV	5.19%	5.65%	5.79%	7.02%	9.63%	9.38%
Subsub-drainage basins	VAR	0.02%	0.08%	0.16%	0.27%	0.55%	0.40%
	STDEV	1.21%	2.29%	2.81%	3.55%	5.40%	4.98%

A.2.2 Results

The relationship between month-averaged river width and month-averaged flow in major WS1 was observed to be poorly defined upon analysis. To analyze the relationship, the slope of width versus flow exceedance was determined for each database point. The relationship was expected to be negative as river width should theoretically increase as flow, and by association flow exceedance, increases. For the entirety of major WS1, 56% datapoints produced a positive slope between width and flow exceedance and 44% produced a negative slope. This result is visualized spatially in Figure 23. For points with width below 100m, 60% produced positive slope relationship and 40% produced negative slope relationship. For points with widths above 100m, 54% produced a positive slope relationship and 46% produced a negative slope relationship. Based on this analysis, it was not expected that WDCs could be produced with confidence. The cloud cover filter was further reduced to nearly 0% to understand if the errors in width caused by cloud cover could be contributing to the poor width to flow exceedance relationship. Upon applying this restricted filter and reanalyzing the width and flow exceedance relationship, the relationship was still found to be poor with approximately 50% of points with a positive slope and 50% with a negative slope. As such, the mean of the month-averaged imagery-derived widths was used to calculate the VDC and HK power in major WS1. An upper power estimate was provided by applying the minimum imagery-derived width for each datapoint location, and a lower power estimate was provided by applying the maximum imagery-derived width for each datapoint location. A spatial relationship may exist between slope and size of the river (i.e., weaker width-exceedance relationships for smaller rivers) or slope and surficial geology (i.e., weaker width-exceedance relationships in bedrock rivers and stronger relationships in sand bed rivers), but this spatial relationship will not be explored in this work.

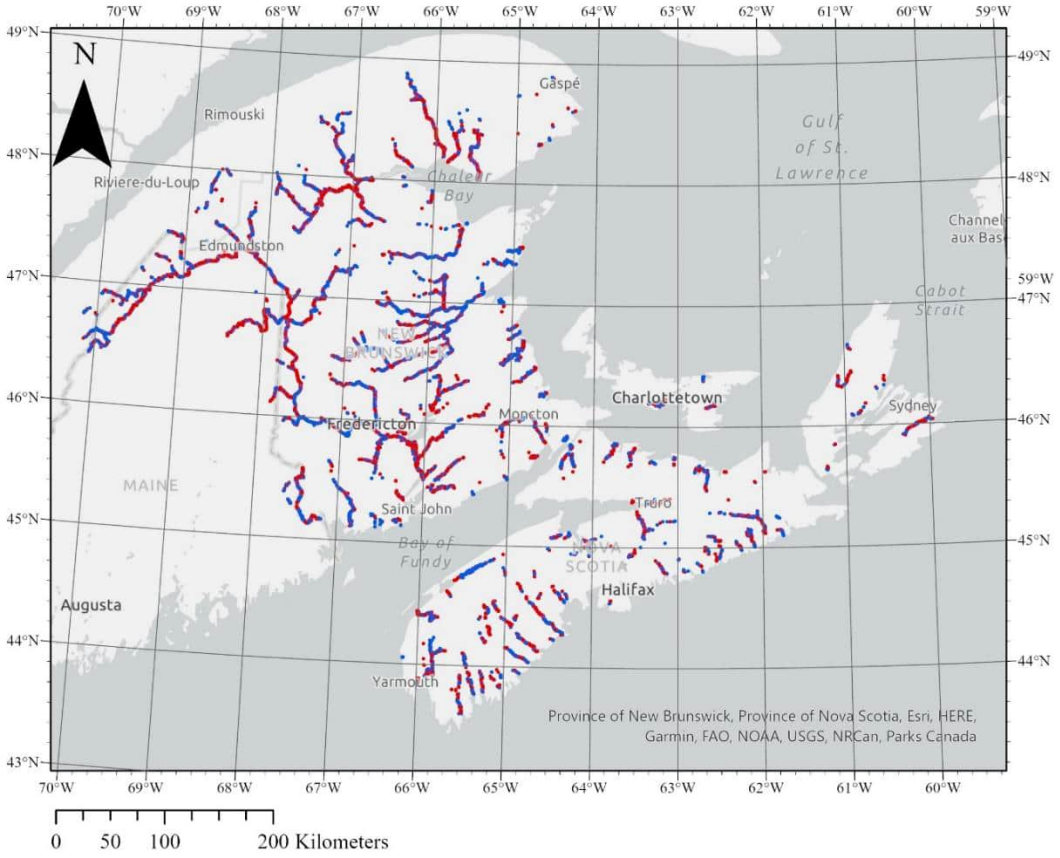

Figure 23: Points with a negative (red) relationship between flow exceedance and width and points with a positive (blue) relationship between flow exceedance and width.

Appendix B

B.1 Hydrokinetic power estimates in selected watersheds

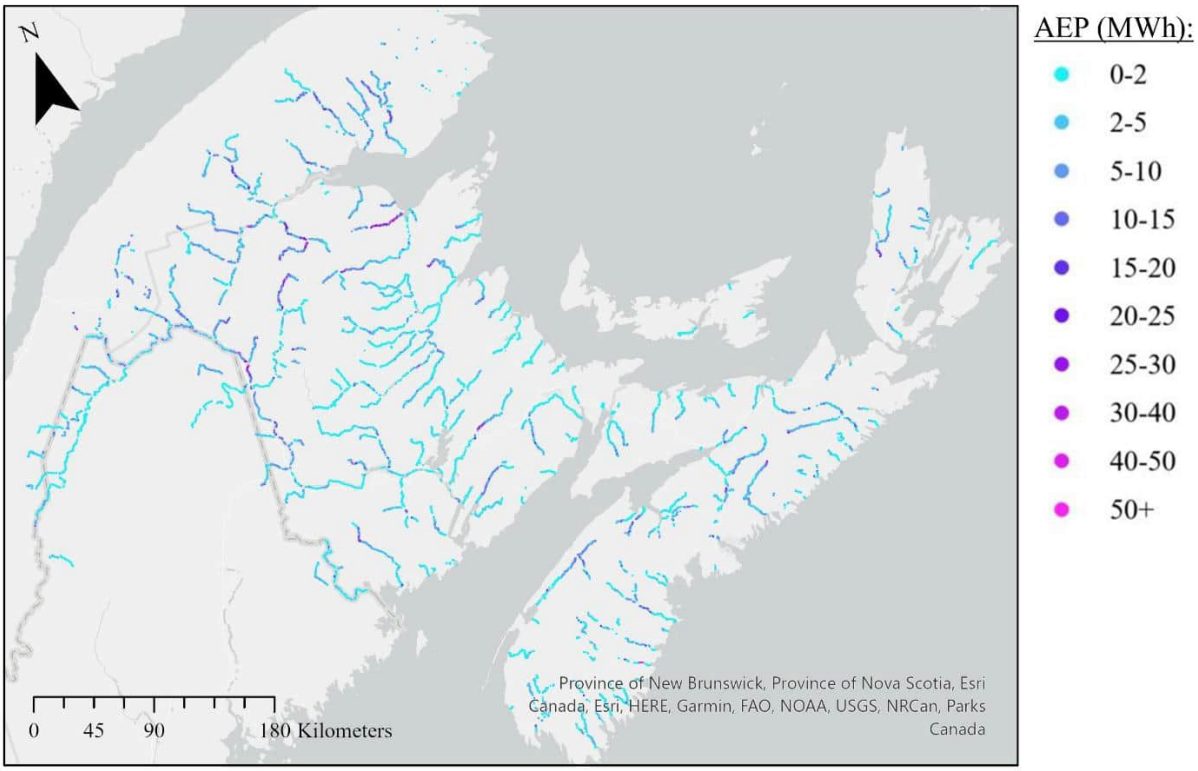

Figure 24: Hydrokinetic power estimates in NHN watershed 01.

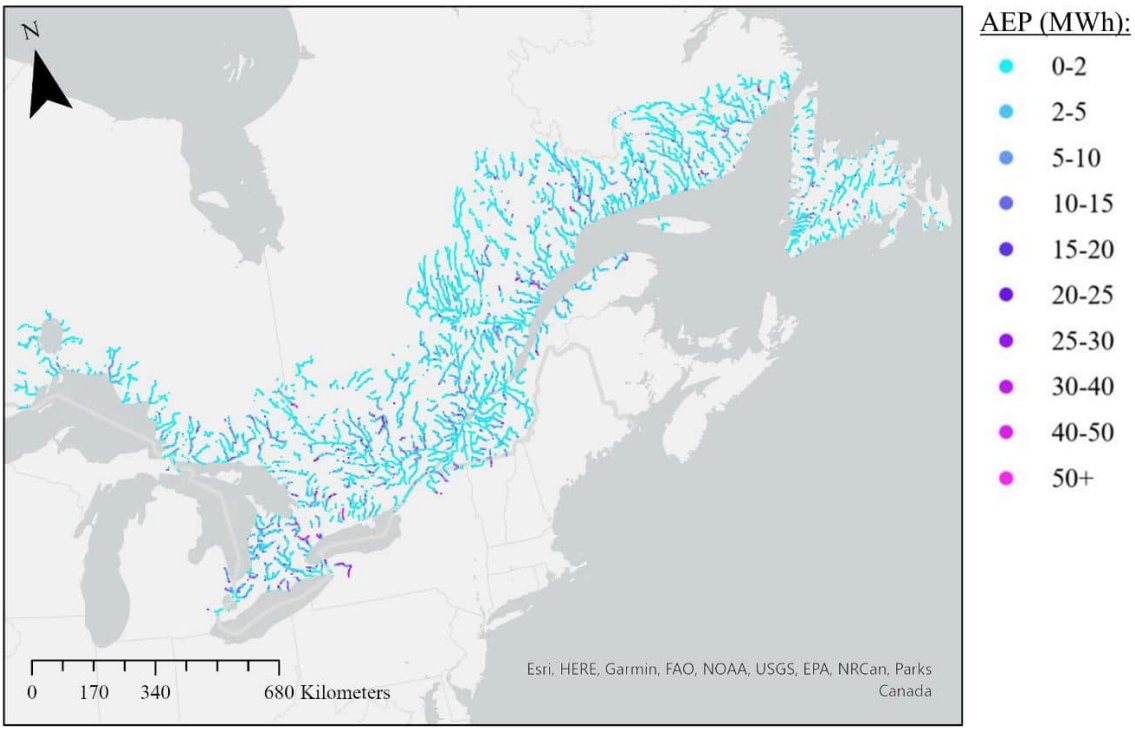

Figure 25: Hydrokinetic power estimates in NHN watershed 02.

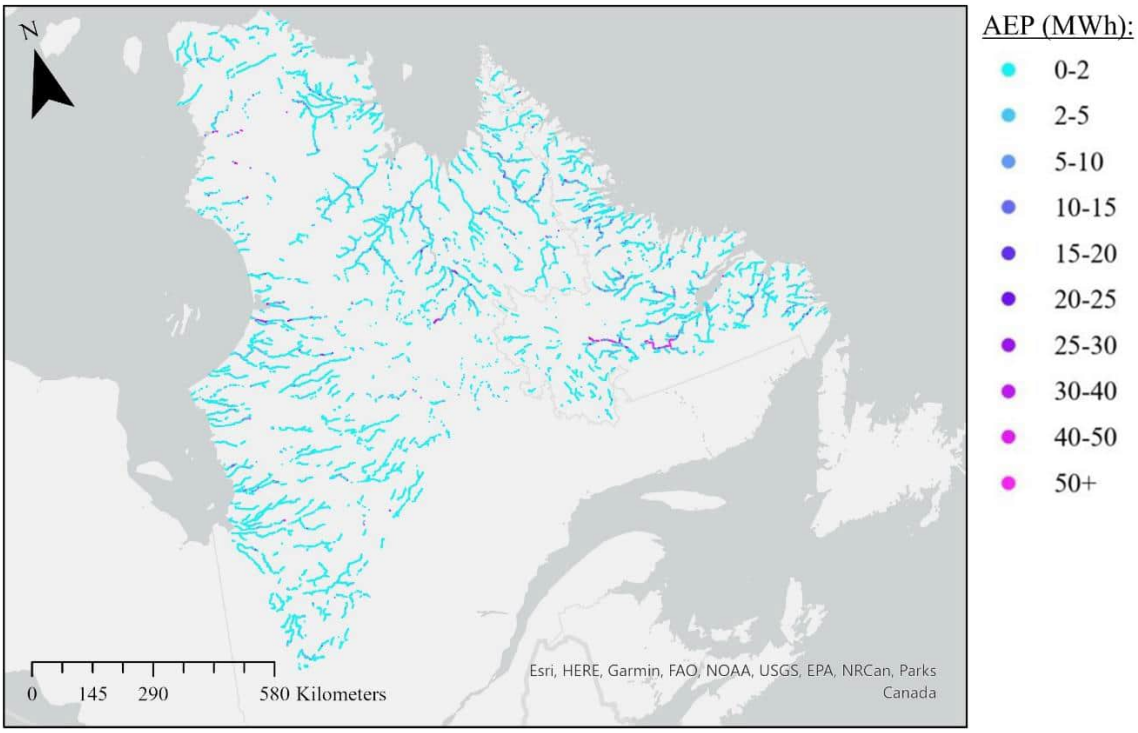

Figure 26: Hydrokinetic power estimates in NHN watershed 03.

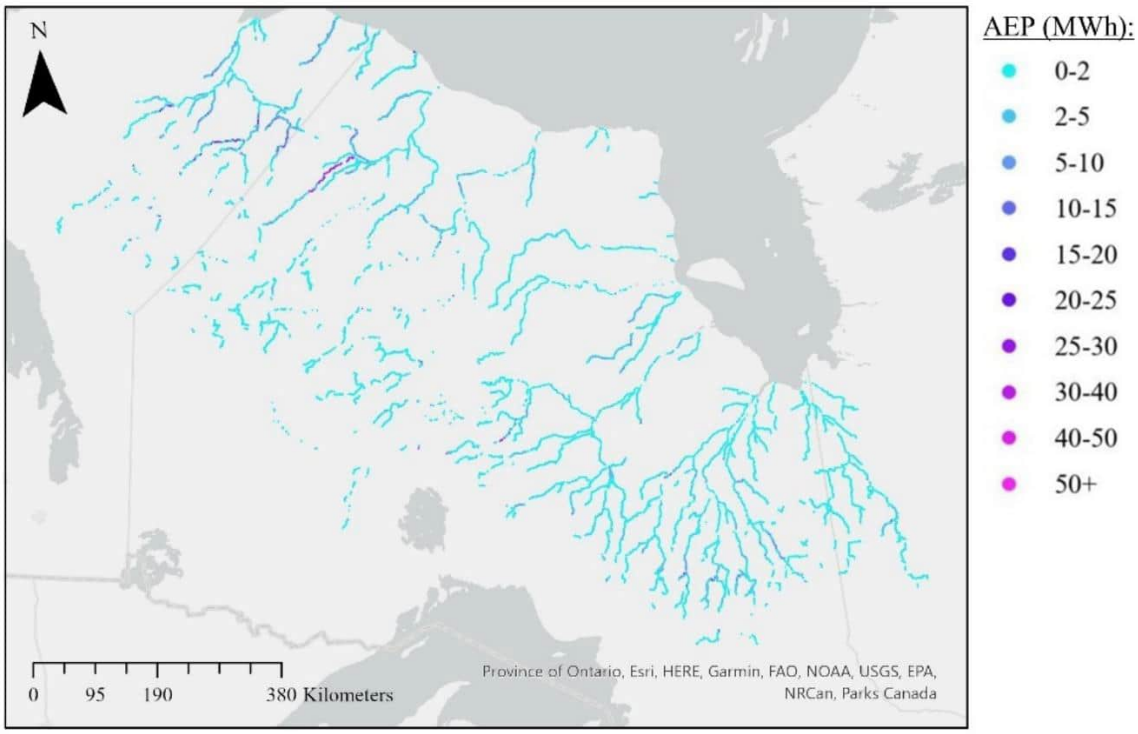

Figure 27: Hydrokinetic power estimates in NHN watershed 04.

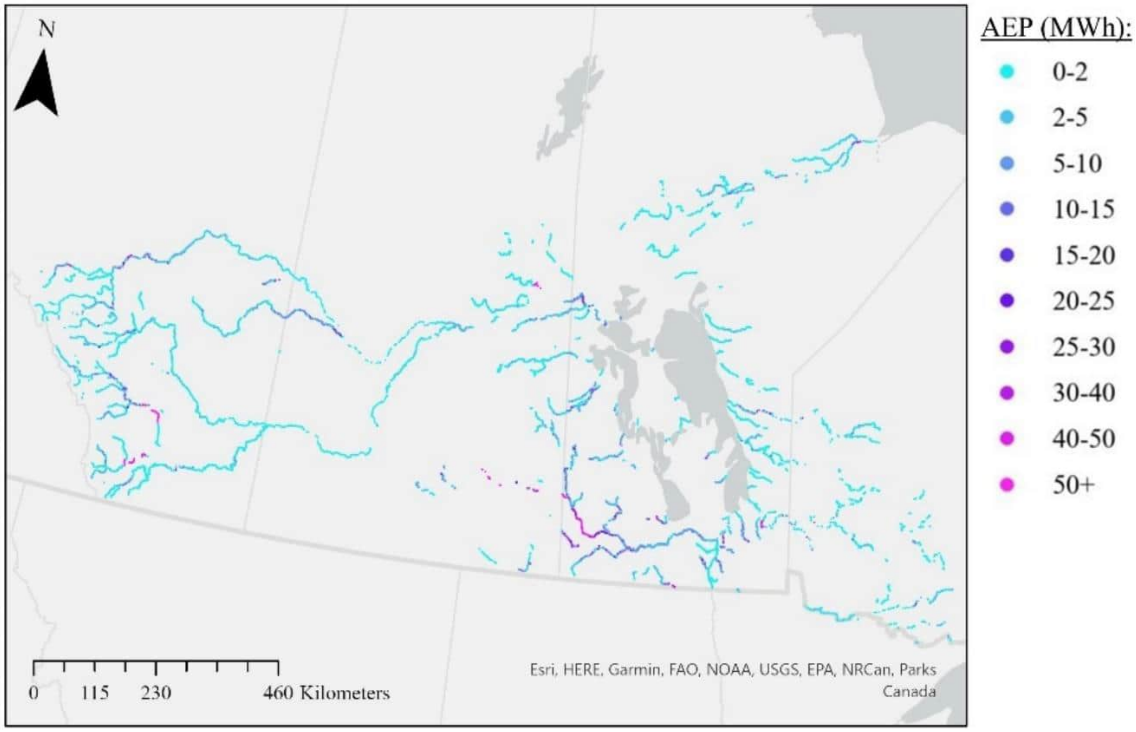

Figure 28: Hydrokinetic power estimates in NHN watershed 05.

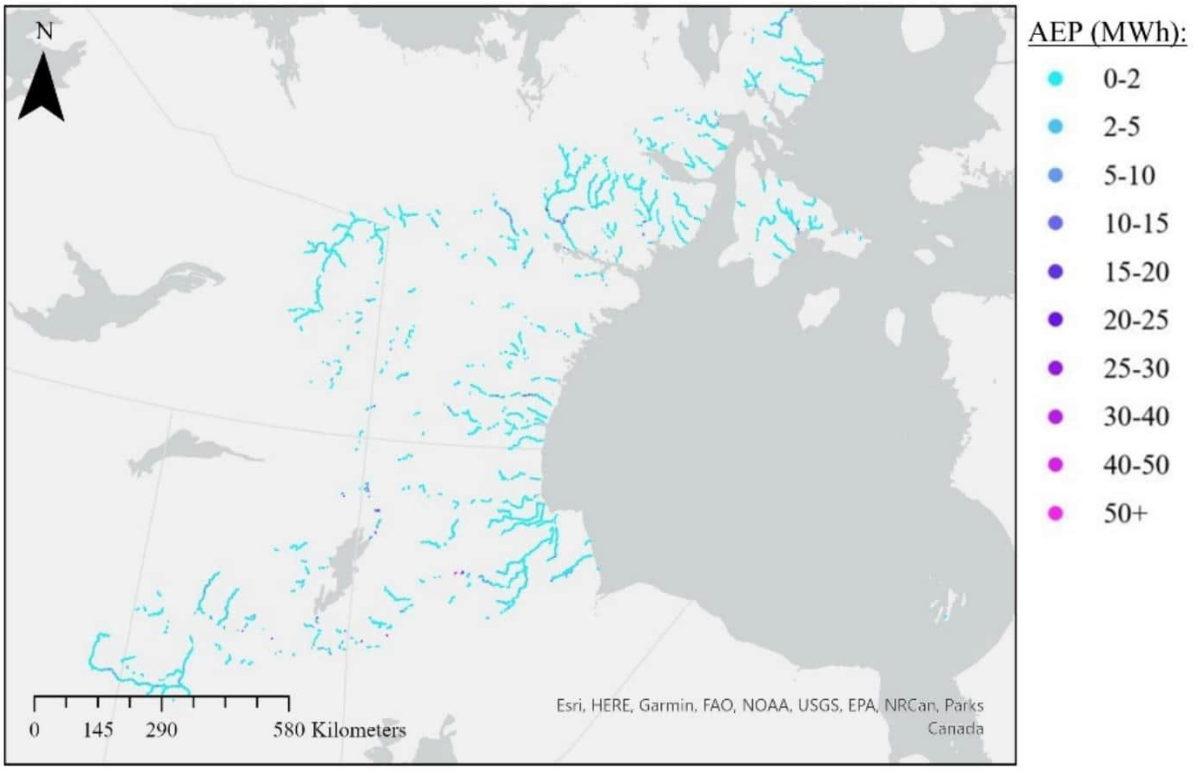

Figure 29: Hydrokinetic power estimates in NHN watershed 06.

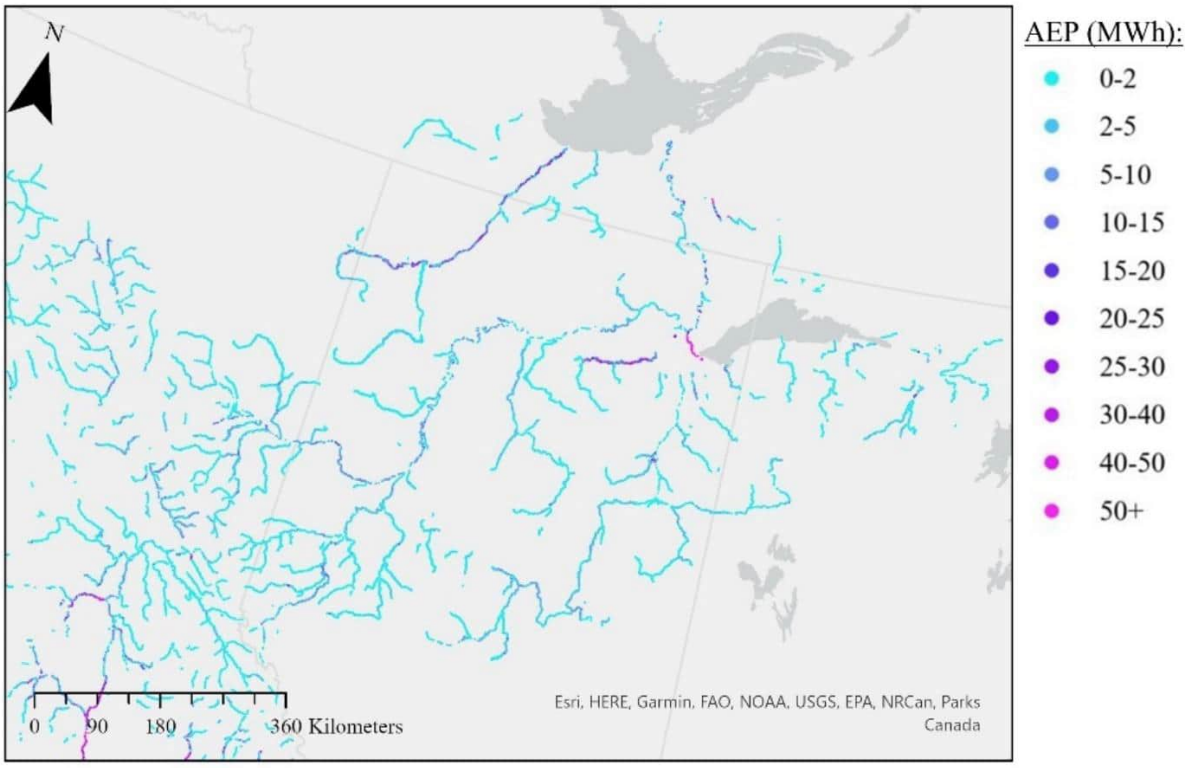

Figure 30: Hydrokinetic power estimates in NHN watershed 07.

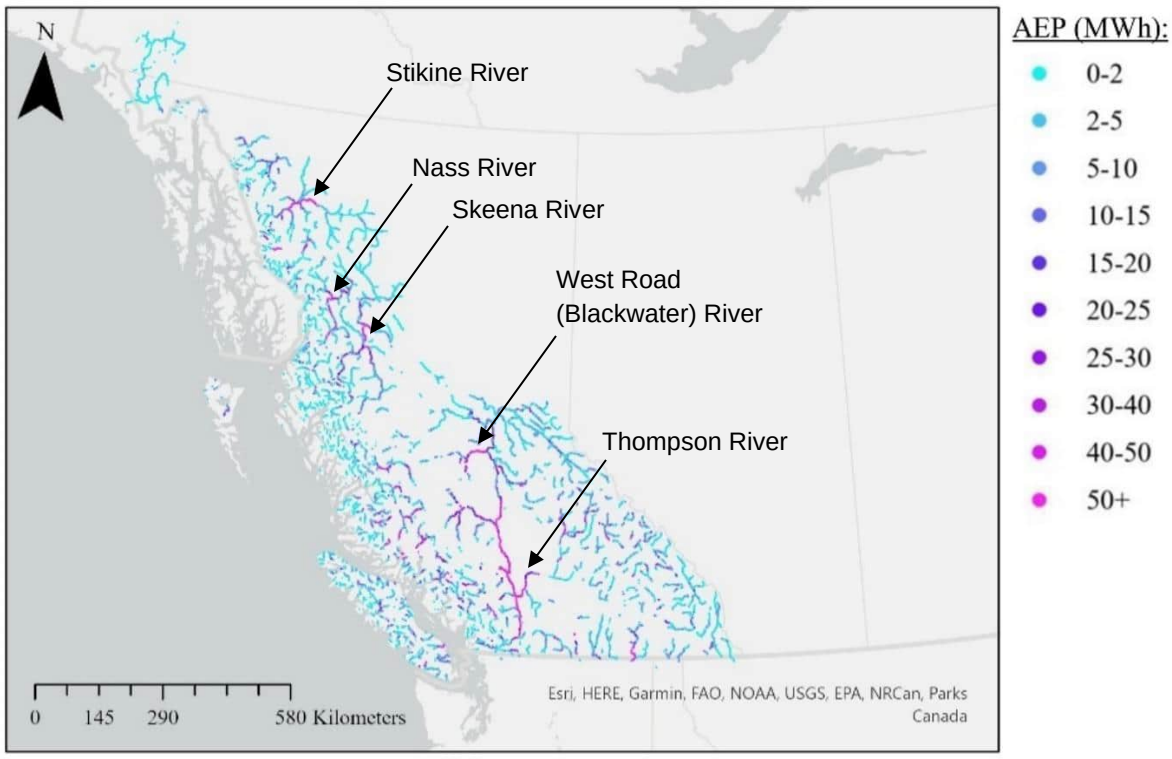

Figure 31: Hydrokinetic power estimates in NHN watershed 08.

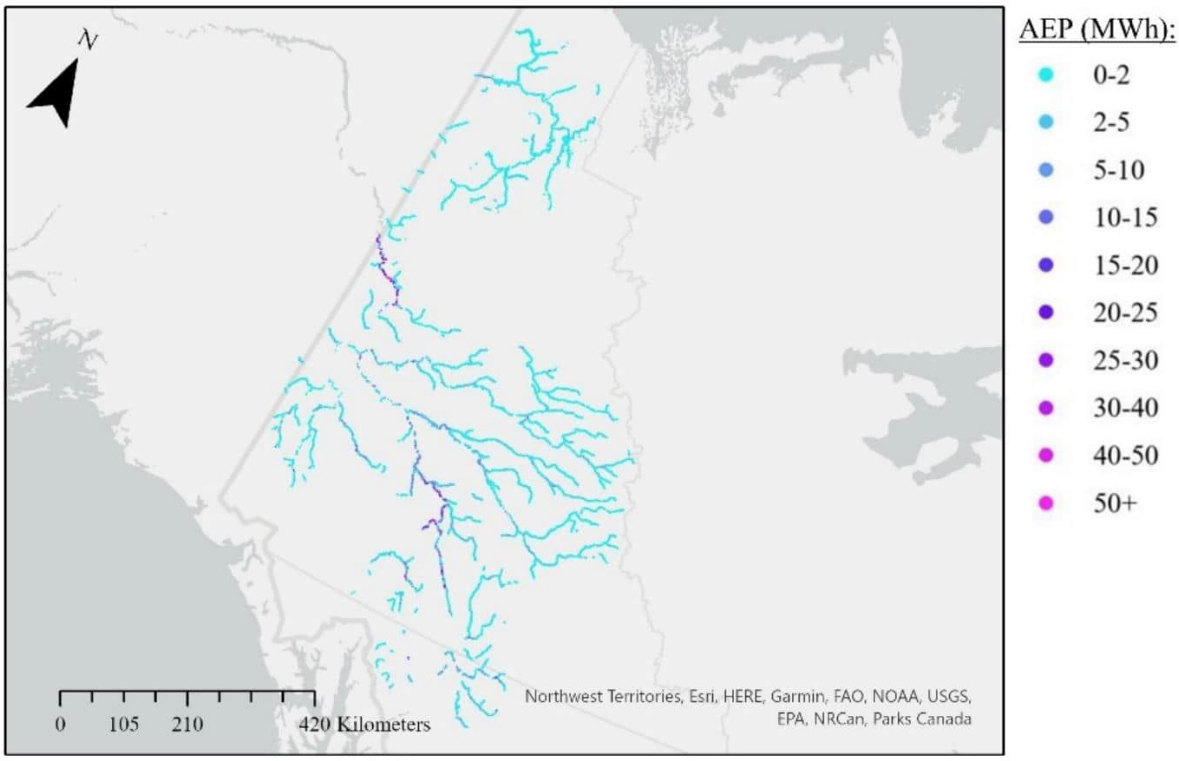

Figure 32: Hydrokinetic power estimates in NHN watershed 09.

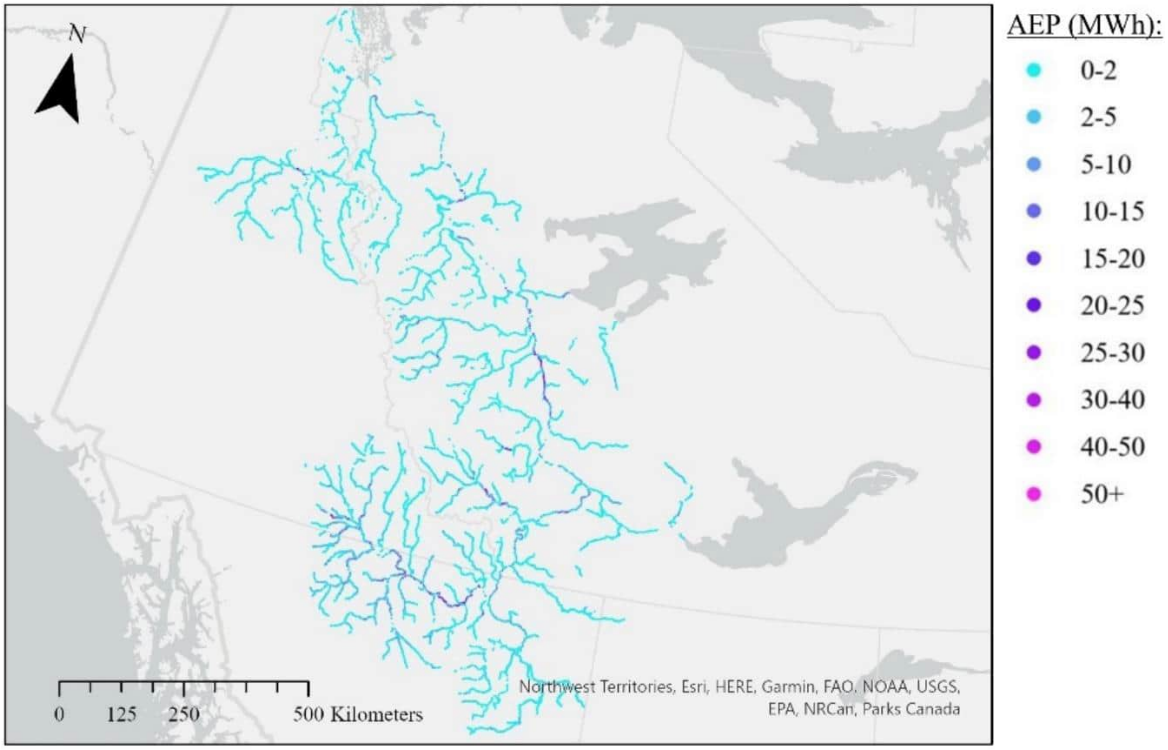

Figure 33: Hydrokinetic power estimates in NHN watershed 10.

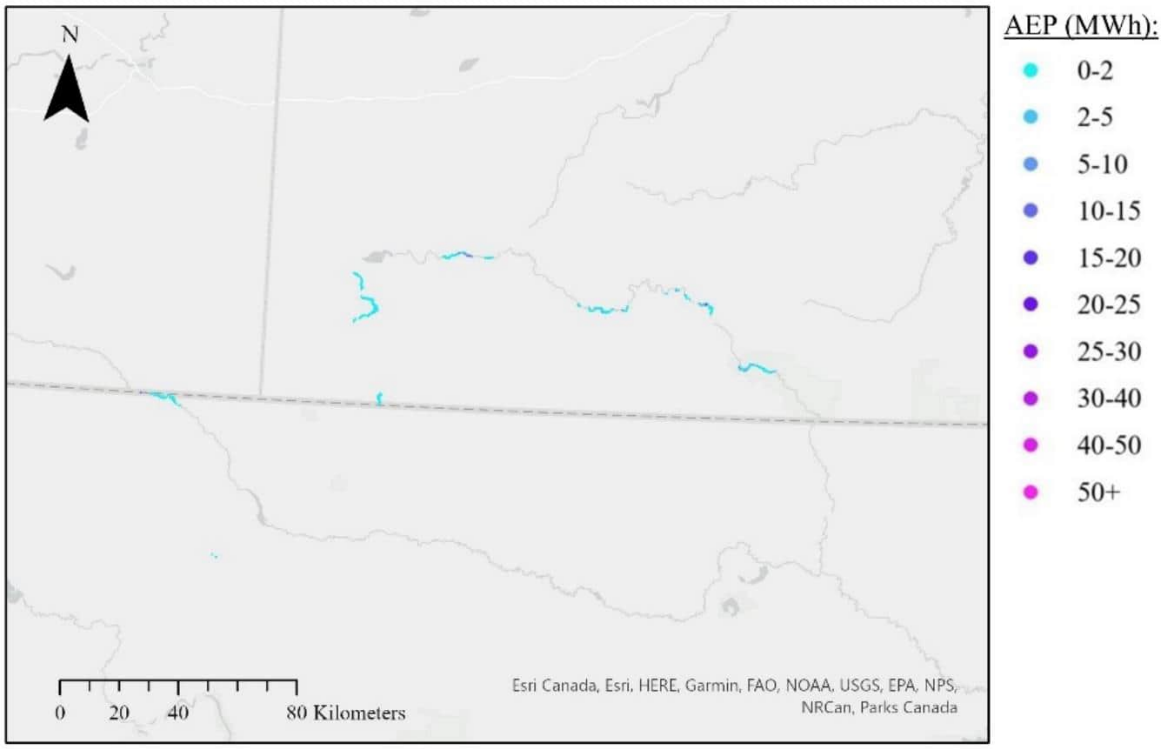

Figure 34: Hydrokinetic power estimates in NHN watershed 11.

National Research Council Canada
Conseil national de recherches Canada

Canada